Ore Geology Reviews 136 (2021) 104285

Contents lists available at ScienceDirect

Ore Geology Reviews

journal homepage: www.elsevier.com/locate/oregeorev

Review

Phase relations of arsenian pyrite and arsenopyrite

Aleksandr S. Stepanov [a,*], Ross R. Large [b], Ekaterina S. Kiseeva [c,d], Leonid V. Danyushevsky [b], Karsten Goemann [e], Sebastien Meffre [b], Irina Zhukova [a], Ivan A. Belousov [b]

[a] Collaborative Innovation Center for Exploration of Strategic Mineral Resources, Faculty of Earth Resources, China University of Geosciences, Wuhan 430074, China
[b] CODES Centre for Ore Deposit and Earth Sciences, Private Bag 126, University of Tasmania, Hobart, TAS 7001, Australia
[c] School of Biological, Earth and Environmental Sciences, University College Cork, T23 N73K, Ireland
[d] Department of Earth Sciences, University of Oxford, Oxford OX1 3AN, UK
[e] Central Science Laboratory, Private Bag 74, University of Tasmania, Hobart, TAS 7001, Australia

ARTICLE INFO

Keywords:
Pyrite
Orogenic gold deposits
Arsenopyrite
Experimental petrology
Sulfide geochemistry
Metamorphism of ore deposits

ABSTRACT

Arsenian pyrite containing above 1 wt% As plays a crucial role in deposition and deportment of Au and other chalcophile elements. The importance of arsenian pyrite led to theoretical and experimental studies that examined properties and genesis of the mineral; however, the interpretation of the phase relations between arsenian pyrite and arsenopyrite is conflicting. In this contribution, we present the results of a review of the experimental studies that have investigated the crystallisation of pyrite in As-bearing systems, a summary of As content in pyrite coexisting with arsenopyrite in 37 deposits and the composition of arsenian pyrite in deposits with little or no arsenopyrite. The review demonstrates that the previous experimental studies that attempted to achieve equilibrium between pyrite and arsenopyrite observed from <1 to 4.7 wt% As in pyrite. The literature survey of the assemblages of pyrite and arsenopyrite shows that pyrite crystallising together with arsenopyrite commonly has a very heterogeneous composition with As content varying from below detection to about 10 wt% As and no clear discontinuities were observed across this range. In the deposits without arsenopyrite, arsenic content in pyrite can reach 20 wt% As. We consider three principal scenarios of the relations of arsenian pyrite and arsenopyrite: (A) Pyrite with high As content is stable in equilibrium with arsenopyrite. Low-As pyrite coexisting with arsenopyrite is a product of disequilibrium crystallisation; (B) a scenario of control of As content in pyrite coexisting with arsenopyrite by thermodynamic parameters including temperature, pressure, the activity of components and fluid composition and (C) a scenario where arsenian pyrite is a metastable mineral. The observations are inconsistent with a model of 5–6 wt% As in pyrite coexisting with arsenopyrite in equilibrium (scenario A). The stability range of the assemblage of pyrite and arsenopyrite constrains the thermodynamic control on the composition of pyrite crystallising in equilibrium with arsenopyrite (scenario B). The scenario of metastable crystallisation of arsenian pyrite (C) proposes formation of the mineral by fast growth from oversaturated fluids with As content controlled by surface adsorption and can explain such features as sector zoning of the mineral and the apparent negative temperature dependence of the solubility. The data phase relations of arsenian pyrite highlight the need for new experimental studies, and suggest that the scenario of disequilibrium phase relations of arsenian pyrite should be considered for interpretation of natural assemblages.

1. Introduction

Pyrite is the most abundant sulfide in the Earth's crust and characterised by wide variations in composition (Abraitis et al., 2004; Deditius et al., 2014; Gregory et al., 2015). One of the most abundant impurities in pyrite is arsenic (As), and pyrite with As content above about 1 wt% As is commonly referred to as arsenian pyrite (Wells and Mullens, 1973). The recognition of the economic importance of arsenian pyrite came in the 1970 s, when studies demonstrated that this mineral could be the principal host for invisible, refractory Au (Wells and Mullens, 1973; Fleet et al., 1988, 1993; Morishita et al., 2018), and As could enhance the uptake of gold and other trace elements into pyrite in hydrothermal ore deposits (Fleet et al., 1988; Huston et al., 1995; Fleet and Mumin, 1997; Reich et al., 2005; Deditius et al., 2014; Peterson and Mavrogenes,

* Corresponding author.
E-mail address: aleksandr@cug.edu.cn (A.S. Stepanov).

https://doi.org/10.1016/j.oregeorev.2021.104285
Received 31 January 2021; Received in revised form 27 May 2021; Accepted 3 June 2021
Available online 6 June 2021

2014; Xing et al., 2019a; Large and Maslennikov, 2020). In addition to its economic importance, arsenian pyrite plays a significant geochemical role, hosting poisonous As that can release into the environment during metamorphism, ore mineral processing and weathering (Large et al., 2007; Pitcairn et al., 2006; Savage et al., 2000).

Despite the economic and geochemical importance of arsenian pyrite, the phase relations of arsenian pyrite in the Fe-As-S system, are still a matter of debate (e. g. Stepanov, 2019; Xing et al., 2019a, 2019b). The experimental studies performed at high temperature reported low As solubility in pyrite (Clark, 1960; Hem and Makovicky, 2004a), whereas lower temperature experiments produced pyrite and marcasite with 2.9–12.6 wt% As that were interpreted as metastable phases (Fleet and Mumin, 1997). These findings are at odds with the first-principles models proposed that As substituting S can be a stable component in pyrite (Blanchard et al., 2007; Reich and Becker, 2006). Specifically, Reich and Becker (2006) estimated that pyrite with approximately 6 wt % of As should coexist in equilibrium with arsenopyrite but that pyrite with higher As content is metastable and at lower As content, pyrite should be undersaturated in As. These estimates were used to develop models of hydrothermal pyrite deposition that also predicted that only pyrite with a narrow range of As concentrations can coexist with arsenopyrite (Vilor et al., 2014; Xing et al., 2019a). These models are at odds with the observations of natural arsenopyrite-pyrite assemblages which can have wide ranges of As concentrations in pyrite from below several hundred ppm to several wt% (Li et al., 2014; Sung et al., 2009; Wu et al., 2019b). Given the importance of arsenian pyrite, this study reviews the previous studies and discusses different scenarios of the relationship between equilibrium pyrite-arsenopyrite and metastable arsenian pyrite based on the experimental results and natural observations.

2. Samples and methods

As concentrations and substitution mechanisms in pyrite are most commonly analysed by the Electron Probe Microanalyzer (EPMA) and Laser Ablation Inductively Coupled Mass Spectrometry (LA–ICP–MS). Other methods used for the study of As incorporation into the pyrite structure include X-ray absorption spectroscopy (Le Pape et al., 2018; Qian et al., 2013), transmission electron microscopy (Palenik et al., 2004) and secondary ion mass spectrometry (SIMS) (Barker et al., 2009; Chouinard et al., 2005; Morishita et al., 2019). The estimation of the substitution mechanism of As in pyrite requires accurate and precise data on all significant components of pyrite and generally measurements by EPMA equipped with WDS detectors are the most suitable for this purpose, although other methods such as SIMS have been occasionally used to study substitution mechanisms (Chouinard et al., 2005). LA–ICP–MS allows measurement of As concentrations in pyrite over the extensive range of concentrations with low detection limits as long as sufficiently low backgrounds are maintained. However, significant fractionation of S and Fe during ablation of sulfides might hinder the quantification of these elements with the accuracy required for the estimation of substitution mechanisms (Gilbert et al., 2014a, 2014b; Stepanov et al., 2020) and low spatial resolution of LA–ICP–MS precludes observation of small scale variation in As content.

Most of the data used in this study was gathered from the scientific literature but four samples of ores with pyrite and arsenopyrite assemblages from Western Australia are reported for illustration purposes. The four samples have been selected from our collection of ores from >35 Au deposits of Western Australia (Belousov et al., 2016) and are characterised by BSE images and EPMA. The detailed description of these deposits has been provided by Belousov et al. (2016). For these samples BSE images and concentrations of Fe, S, and As were determined by point analyses on a Cameca SX100 EPMA at 20 kV accelerating voltage and 20 nA probe current, using a focussed beam and the Probe Software Inc. for EPMA software package. Counting times on wavelength-dispersive spectrometry detector (WDS) for all elements were 60 s each for both peak and total background. Fe and S were measured using Kα line calibrated on PPP-1 pyrite standard (Gilbert et al., 2014a, 2014b). Arsenic was measured on Lα line and calibrated on GaAs Astimex standard.

3. Results

3.1. Substitution mechanisms of As in pyrite

Pyrite could incorporate As in a variety of substitution mechanisms (Deditius et al., 2014, 2008; Qian et al., 2013). The most widespread substitution mechanism in pyrite is S ⇔As or Fe(S, As)$_2$ (Fleet and Mumin, 1997). Another substitution type Fe ⇔As or (Fe, As)S_2 has been observed in the Yanacocha deposit and in synthetic pyrite (Deditius et al., 2008; Le Pape et al., 2018; Qian et al., 2013). The presence of trace element nanoparticles (Deditius et al., 2011) and nanoscale "liquid" inclusions of As–Fe–S has been reported in pyrite from some deposits (Deditius et al., 2009). Coupled substitutions (Fe,$As_{0.5}Ag_{0.5}$)S_2 and (Fe, $As_{0.5}Cu_{0.5}$)S_2 have been observed in the Pascua epithermal deposit (Chouinard et al., 2005). Pyrite with the substitution Fe(S,As)$_2$ is formed at reduced conditions such as orogenic gold deposits hosted by sediments, whereas substitution (Fe, As)S_2 was observed at the oxidised conditions in epithermal deposits (Deditius et al., 2008; Kusebauch et al., 2018a; Qian et al., 2013).

3.2. Experimental data on As in pyrite

The synthesis of pyrite in As-bearing systems has been achieved by different experimental techniques (Table 1). The duration of the experiments varied from several hours to about a year. Some studies attempted to achieve equilibrium and employed such techniques as long experimental runs with additional rounds of regrinding and annealing, and the addition of fluxes to increase reaction rates (Barton, 1969; Clark, 1960; Hem and Makovicky, 2004a; Kretschmar and Scott, 1976). Other studies aimed to reproduce the natural hydrothermal processes and performed experiments over shorter periods (Fleet and Mumin, 1997; Kusebauch et al., 2018a; Qian et al., 2011).

Clark (1960) performed experiments on pyrite in evacuated silica glass tubes at 500–600 °C and estimated that at 600 °C, pyrite coexisting with pyrrhotite and the sulfur-arsenic liquid contained just under 0.53 wt% As (Fig. 1a). The dissolution of As in pyrite was proposed based on the decreasing pyrrhotite content in the assemblage. One of the principal features of the system discovered by Clark (1960) was a reaction of pyrite and arsenopyrite producing pyrrhotite (Fig. 2). The temperature of this reaction was closely bracketed at 491 ± 12 °C (Fig. 2) by using long high-temperature runs and a magnet for identification of the first appearance of pyrrhotite (Barton, 1969). These and additional experiments in the Fe-As-S system allowed Barton (1969) to propose the first thermodynamic model of the system.

Arsenopyrite, a principal mineral in As-bearing assemblages, often described by the formula FeAsS, but it has variable contents of As and S and hence should be described as Fe(As, S)$_2$ or FeAs(As, S). The dependence of the arsenopyrite composition on various parameters has been studied by Kretschmar and Scott (1976) who used two types of experiments: dry experiments with only Fe-S-As phases present and experiments with the addition of mixtures of halides with low melting temperatures that increased the reactions' speed. The later study by Sharp et al. (1985) considered the effect of pressure on arsenopyrite phase relations. These studies have not reported compositions of pyrite in experimental products, possibly due to the heterogeneity of this mineral. The experiments in the Ni-Co-Fe-As-S system at 500 °C produced zoned Ni and Co-bearing pyrite with 0.1–4.5 at% As characterised by Fe(S,As)$_2$ substitution in equilibrium with monosulfide solid solution, arsenopyrite and other high-As phases (Fig. 3a) (Hem and Makovicky, 2004a). The average compositions of pyrite varied from 1.3± 0.9 wt% As to 4.7± 1.6 wt% As. These experiments involved several cycles of annealing for 3–4 months, regrinding and repeated annealing. The total

Table 1
A summary of conditions of the experimental studies performed in As-bearing systems with pyrite.

Reference	Temperature	System/components	Duration
Clark (1960)	400–750 °C	Fe-As-S	5–304 days
Barton (1969)	281–825 °C	Fe-As-S	21–338 days
Kretschmar and Scott (1976)	300–680 °C	• Fe-As-S • Eutectic halides (flux)	4–187 days
Hem and Makovicky (2004a), Hem and Makovicky (2004b)	500–650 °C	• Fe–Co–Ni–As–S • LiCl–KCl flux	3 times 3–4 months with regrounding
Tauson (1999)	500 °C	• Greenockite • Pyrite • H_2O solution NH_4Cl, Au, As	Not reported
Cafagna and Jugo, (2016)	• Fused at 1200 °C (then cooling at 60 °C/h), • 750 °C (then cooling at 0.5 °C/h) • Annealing at 650 °C • quench	• Natural sulfides (pyrrhotite, chalcopyrite, pentlandite) • elemental S • Metalloids and PGE	About 200 h
Fleet and Mumin, (1997)	310–605 °C	• Fe-As-S • H_2O • NaCl and KCl (flux)	5–57 days
Qian et al. (2013)	125–220 °C	• Magnetite • Thioacetamide • Buffer solutions • Various As substance	31 days
Kusebauch et al. (2018a)	200 °C	• Siderite or black shale containing siderite • Pyrite seeds • Thioacetamide • H_2O solution with S and As	22–332 h
Pokrovski et al. (2002)	300–450 °C	• Arsenopyrite • +/- H_3AsO_3 • +/-HCl/NaOH solutions • +/- Py–Po–Mt buffer	1–125 days

duration of the experiments was close to a year, and they represent the best data currently available on the composition of pyrite coexisting with arsenopyrite at conditions close to equilibrium, however the significant heterogeneity of pyrite suggested that pyrite was still less well equlibrated than other phases (Hem and Makovicky, 2004a).

To reproduce crystallisation of sulfides in magmatic systems and to produce larger pyrite crystals, Cafagna and Jugo (2016) synthesised pyrite by multistep cooling of mixtures of Fe-sulfides with chalcophile elements including As (Table 1). The main crystallisation stage at 650 °C was followed by quenching. The synthesised pyrite contained As-rich inclusions and in some experiments coexisted with As-rich sulfide melt with about 7.4 wt% As. Pyrite which crystallised at these conditions contained 260–400 ppm As.

Another type of experimental studies aimed to reproduce the conditions of arsenian pyrite growth in hydrothermal deposits (Table 1). Arsenian pyrite and marcasite were synthesised by Fleet and Mumin (1997) at temperatures of 310–405 °C. The arsenic content of minerals varied from 2.9 to 7.7 wt% As in arsenian pyrite and 10–12.5 wt% As in marcasite synthesised at 310 °C. Marcasite with 16.5 wt% As was observed in an experiment at an unspecified temperature. The compositions of pyrite corresponded to $Fe(S, As)_2$ substitution (Fig. 3a). Using the reaction of S- and As-rich fluids with magnetite at 120–220 °C, Qian et al., (2013) produced pyrite with $(Fe, As)S_2$ substitution and As contents from <0.03 to 23.8 wt%. In the experiments where the source of As was more reduced arsenopyrite or lollingite, the As content in pyrite was lower than in experiments where As was sourced from realgar and compounds with oxidised As, such as As_2O_3 and $Na_2HAsO_4*7H_2O$. Kusebauch et al. (2018) performed experiments on the replacement of siderite by pyrite from As-bearing fluids that produced a wide range of pyrite compositions with up to 7 wt% As and showed systematic variation in As content of pyrite with changes in compositions of starting solutions.

3.3. *Arsenic concentration in pyrite coexisting with arsenopyrite in sulfidic ores*

Assemblages of pyrite and arsenopyrite are widespread in ore deposits and in unmineralised metamorphic rocks (Tomkins et al., 2007). A systematic literature-based data compilation of pyrite composition from arsenopyrite-bearing samples from 37 ore deposits (Table 2) show that this assemblage is common in orogenic gold type, but is sometimes reported in epithermal, gold skarn, Carlin-type and volcanic-hosted massive deposits (Fig. 1b). The ores of WA deposits commonly show evidence of simultaneous crystallisation of pyrite and arsenopyrite (Figs. 3, 4, Table 2, Supplementary Table S1). For example, the ore from the Meekatharra Prohibition deposit contains arsenopyrite both as small inclusions in the zoned pyrite crystals and coarse grains in the silicate and carbonate matrix (Fig. 4). The highest As content of 3.2% occurs in irregular inner zones (Supplementary Table S1), whereas zones containing <260 ppm As occur in direct arsenopyrite crystals (Fig. 4a). The samples of ores from Youanmi and Lancefield deposits are composed of massive fine-grained pyrite intergrown with crystals of arsenopyrite which crystallised together (Fig. 4c–d). While As content in pyrite was variable from <260 pm to 2200 ppm, in the immediate vicinity of arsenopyrite As content reached very low values down to the limit of detection (Fig. 4c–d). A sample from the Paddington deposit is composed of a quartz vein with large (2–3 mm) crystals of pyrite and arsenopyrite that have no immediate contact. The cores of pyrite contain inclusions of pyrrhotite and have negligible As contents (5–35 ppm As by LA-ICP-MS; Belousov et al., 2016). In contrast, the inner rim zones of the pyrites have 1–1.3 wt% As, followed by the rims with 0.2–0.5 wt% As (Fig. 4b).

The deposits with pyrite-arsenopyrite assemblages described in the literature similarly contained multiple generations of pyrite, sometimes several stages of arsenopyrite crystallisation and abundant evidence of the simultaneous crystallisation of the two minerals. While in some deposits the arsenopyrite formed late in the history of the ores (e. g. Boiron et al., 1989), in others the pre-ore stage pyrites, sometimes of sedimentary origin, with low to moderate As concentrations were followed by the stages of co-crystallisation of arsenian pyrite and arsenopyrite (Hou et al., 2016; Large et al., 2007; Li et al., 2014; Zhang et al., 2017). In the epithermal Patricia deposit in Chile pyrite and arsenopyrite crystallised prior and after the main stage of sulfide deposition (Chinchilla et al., 2016) whereas in Kuh-Pang deposit in Iran, pyrite and arsenopyrite crystallisation preceded the deposition of copper sulfides (Rajabpour et al., 2017). In the Gutaishan deposit, China Li et al. (2019) documented crystallisation of arsenopyrite with pyrite during several stages with an increasing abundance of arsenopyrite. The ores from Fairview and Sheba mines in South Africa contained both coarse arsenopyrite and arsenopyrite inclusions in pyrite (Agangi et al., 2014).

The survey of the literature indicates that almost universally pyrite shows heterogeneity in As content that is well outside of the analytical uncertainty. For example, in over 50% of the deposits the difference between the maximum and minimum As content of pyrite coexisting with arsenopyrite is larger than a factor of 10 (Table 2). These observations are consistent with the previous detailed studies of pyrite in ore deposits that demonstrated that the distribution of pyrite compositions could be multimodal and multiple complex correlations of elements commonly occur (Cook and Chryssoulis, 1990; Morey et al., 2008;

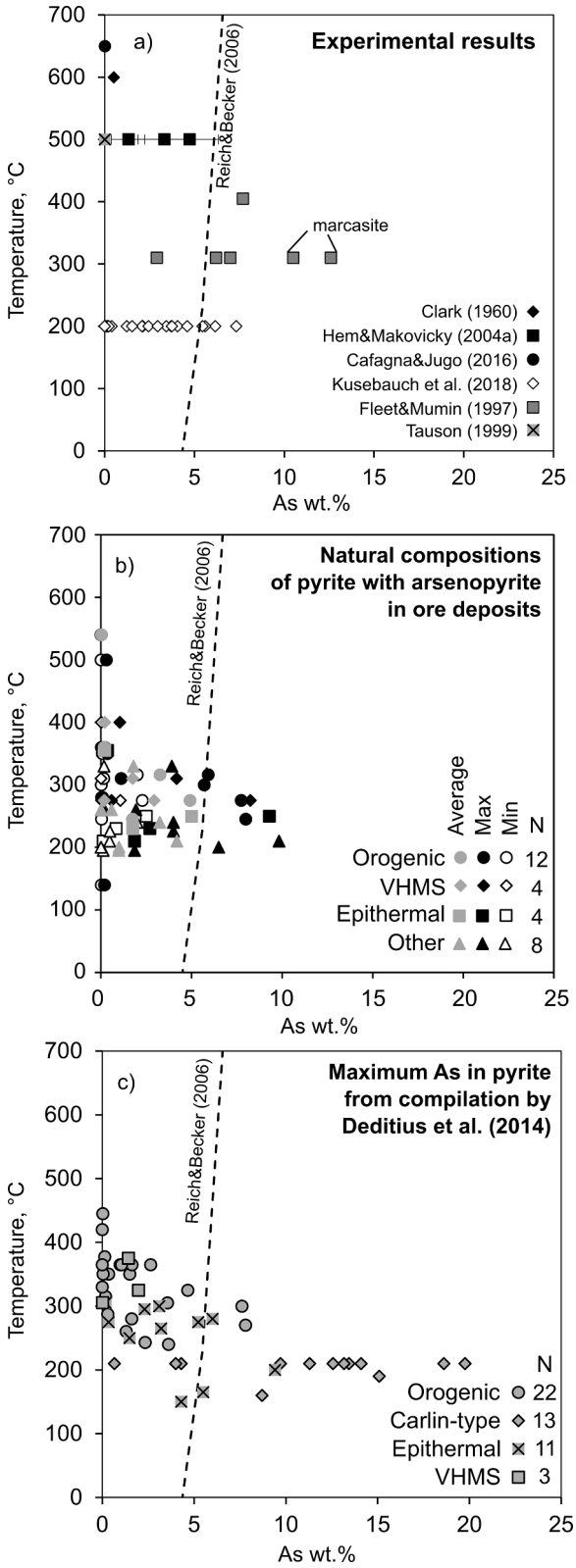

Fig. 1. The compilation on As content in pyrite versus temperature. a) Data from experimental studies. The solubility of As in pyrite in equilibrium with arsenopyrite calculated by Reich and Becker, (2006) is shown by dashed line. b) As content in pyrite coexisting with arsenopyrite from different types of ore deposits. The data sources are listed in Table 2 and the number of deposits in each category is provided as N. c) Maximum As concentrations in pyrite from various ore deposits compiled by Deditius et al. (2014) and typically in assemblages without arsenopyrite. The references are provided in Supplementary Table S2.

Sykora et al., 2018; Winderbaum et al., 2012). Arsenic variations in pyrite may occur on submicron to nano-scale levels (Peterson and Mavrogenes, 2014; Wu et al., 2019b). For multimodal populations, the average values could be unrepresentative and arithmetic mean, geometric means and median could differ significantly while the standard deviation could be an inadequate measure of the dispersion. The great diversity in the pyrite compositions reported in different studies complicates the comparison of the observations. Therefore, in order to better show the compositional variations reported by different studies, we chose to report the highest, lowest and the average As content of pyrite coexisting with arsenopyrite in Fig. 1b and Table 2. The pyrite compositions reported in many papers are not suitable for proper evaluation of the mechanism of substitution of As in pyrite due to incomplete analysis or insufficient precision on Fe and S concentrations. However, where the substitution mechanism was investigated (Fig. 3), the $Fe(S, As)_2$ substitution was observed (Agangi et al., 2014; Li et al., 2014; Zacharias et al., 2004). Overall, a broad trend of As content increasing with decreasing temperature is apparent in the dataset and also apparent in the experimental data. A somewhat similar trend has been observed by (Deditius et al., 2014) in the dataset of average As concentrations in pyrite from various deposits.

3.4. *Arsenic concentrations in arsenian pyrite*

As a mineral, arsenian pyrite is commonly observed in deposits without or with very little arsenopyrite (Simon et al., 1999a). Such assemblages could represent As-undersaturated systems (e. g. Xing et al., 2019a, 2019b) and therefore, we compare here As content in pyrite from these type of ores. For this purpose, we used the list of deposits by Deditius et al. (2014) which, in most cases, did not contain significant amounts of arsenopyrite and plotted the data as the maximum As content versus the temperature of mineralisation (Fig. 1c).

Arsenian pyrite has been reported from several deposit types including orogenic gold, VHMS, Carlin-type, epithermal and deposits with transitional characteristics (Supplementary Table S2). Pyrite commonly has a highly heterogeneous As distribution with oscillatory and sector zoning (Fig. 5). In orogenic type deposits the As content in pyrite can reach 7.6 wt% As, similar to the values we found in orogenic gold deposits with arsenopyrite (Table 2). Arsenian pyrite occurs in epithermal type deposits where it forms at temperatures 150–305 °C (Table 2). The As content in pyrite in epithermal deposits is highly variable and can reach up to 9.4 wt%. The pyrites with highest As concentrations reaching 10–20 wt% occur in Carlin-type gold deposits formed at temperatures close to 200 °C (Barker et al., 2009; Gopon et al., 2019; Reich et al., 2005; Simon et al., 1999b). The potential of the presence of micro inclusions of arsenopyrite in pyrite analyses with extremely high As concentrations should not be overlooked, substitution $Fe(S, As)_2$ is characteristic for Carlin-type deposits (Deditius et al., 2014; Reich et al., 2005).

4. Discussion

Reich and Becker (2006) predicted a bell-shaped solvus between pyrite-arsenopyrite and estimated a slight decrease of As from about 6 wt% As in pyrite in equilibrium with arsenopyrite at 450 °C (Fig. 1a) to about 5 wt% As at 200 °C. Below these values, the solid solution should be undersaturated and above, the solid solution was interpreted to be metastable. Based on the diagram by Reich and Becker (2006), subsequent studies have developed thermodynamic models for hydrothermal As-bearing systems that predicted that pyrite with <5 wt% As cannot be in equilibrium with arsenopyrite (Vilor et al., 2014; Xing et al., 2019a).

Judging by the experimental data and studies of natural sulfidic ores

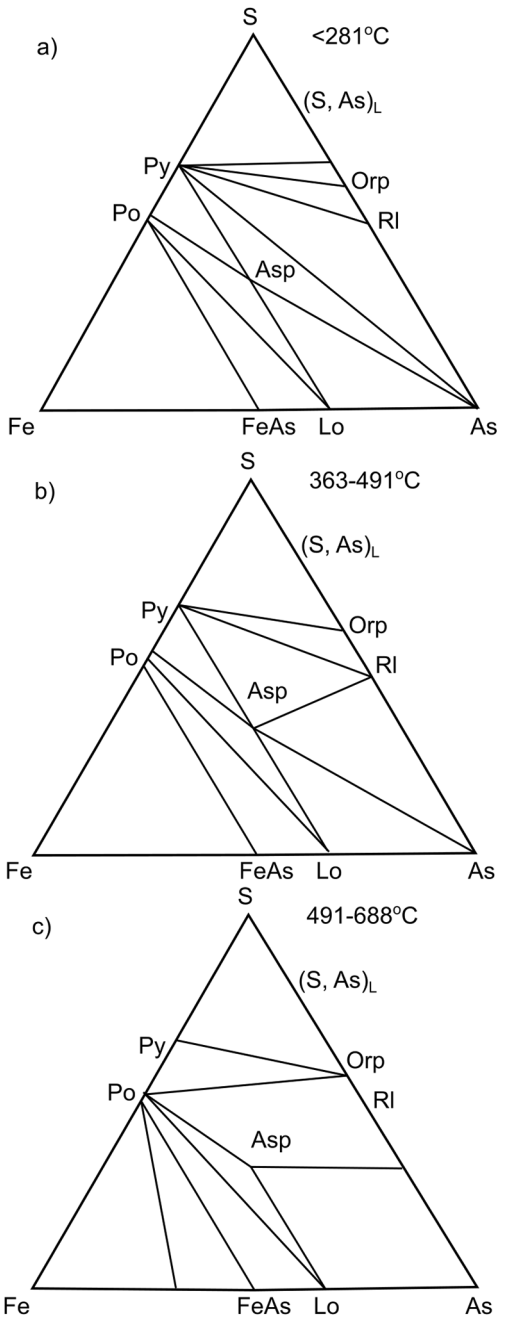

Fig. 2. Simplified sections through dry Fe-As-S system (Clark, 1960; Kretschmar and Scott, 1976). At low temperatures (a) pyrite could coexist with a variety of hgh-As phases though these assemblages rarely occur in nature. The temperature range between 281 and 491 °C (b) represent typical conditions of the assemblage of pyrite and arsenopyrite. The principal reaction occurs at 491 °C above which (c) assemblage of pyrite and arsenopyrite is no longer possible. Asp – arsenopyrite, Py – pyrite, Po – pyrrhotite, Lo – lollingite, $(S, As)_L$ – sulfur –arsenic liquid/melt, Orp–orpiment and Rl–realgar.

summarised above, we conclude that these models fail to reproduce the following key observations:

- Experiments estimated that, in pyrite in equilibrium with arsenopyrite and other high-As phases, arsenic solubility in pyrite is below 1 wt% (Cafagna and Jugo, 2016; Clark, 1960; Tauson, 1999) and 1.3± 0.9 wt% As to 4.7± 1.6 wt% As (Hem and Makovicky, 2004a,b) (Fig. 1a) Hem and Makovicky (2004a), Hem and Makovicky (2004b).
- Pyrite occurring with arsenopyrite in nature has widely variable As content (Fig. 1b) with the maximum As content reaching 6–10 wt% As. In the majority of cases, arsenic content is significantly lower than these values and the lowest reported As content in pyrite coexisting with arsenopyrite for all the compiled ore deposits is <3 wt% (Fig. 1, Table 2).
- Arsenopyrite can coexist at distances of several microns or in direct contact with pyrite containing <400 ppm As (Fig. 4).
- In deposits where arsenopyrite is absent, the highest As contents of 10–20 wt% As have been reported, whereas in arsenopyrite-bearing assemblages, arsenic content in pyrite is <10 wt% (Fig. 1c).
- A negative temperature dependence of As content in pyrite is apparent in the experimental data and natural occurrences of pyrite (Fig. 1).

Several scenarios of the phase relationship between pyrite and arsenopyrite are proposed (Fig. 6):

- Scenario A) Pyrite with high As content is stable in equilibrium with arsenopyrite. Low-As pyrite coexisting with arsenopyrite is a product of disequilibrium crystallisation.
- Scenario B) As content in pyrite coexisting with arsenopyrite in equilibrium depends on the thermodynamic conditions (p, T, fO_2, fluid composition).
- Scenario C) Arsenian pyrite (i. e. pyrite with high As) is formed by disequilibrium crystallisation and could represent a metastable phase.

In the following sections we compare these scenarios with the observations and investigate their implications.

4.1. Scenario A: Arsenian pyrite is formed in equilibrium with arsenopyrite

Vilor et al. (2014) and Xing et al. (2019a), Xing et al. (2019b) have developed models of the behaviour of the arsenian pyrite in hydrothermal systems by fitting the thermodynamic parameters to data of Reich and Becker (2006). Unfortunately, the predictions of these models are in disagreement with the widespread coexistence in nature of arsenopyrite and pyrite with As content much lower than 5–6 wt% (Fig. 1b) and the experimental studies (Fig. 1a). Moreover, our review and study of natural samples from various sulfide deposits (Table 2) failed to find a single example of an assemblage of arsenopyrite and homogeneous pyrite with 5 or 6 wt% As that is predicted in this scenario.

Xing et al. (2019b) proposed that coexistence of low-As pyrite with arsenopyrite could be explained by disequilibrium crystallisation of the minerals, although they did not specify details. One such mechanism could be the crystallisation of arsenopyrite and low-As pyrite from separate batches of fluids with different As content, however, it contradicts the numerous observations of simultaneous crystallisation of arsenopyrite with low-As pyrite (e. g. Agangi et al., 2014; Fig. 4c, d). In this scenario, fluids entering rocks that contain arsenopyrite and pyrite should be able to dissolve arsenopyrite and produce pyrite with increasing As content, which is not supported by the observations. Another disequilibrium pathway could require crystallisation of low-As pyrite from solutions with high As content. This mechanism does not seem geologically likely as the formation of an oversaturated solid solution is much more common than undersaturated solid solutions (e. g. Watson, 1996).

If the assemblage of low-As pyrite and arsenopyrite occurs at disequilibrium, as proposed by Xing et al. (2019b), then the metamorphism or recrystallisation of these mineral assemblages should result in the evolution of the system to equilibrium compositions: that is to the dissolution of arsenopyrite in pyrite, the diffusion of As into pyrite and the development of As-rich haloes around arsenopyrite inclusions in pyrite. Such textures have not been documented in the literature. On the

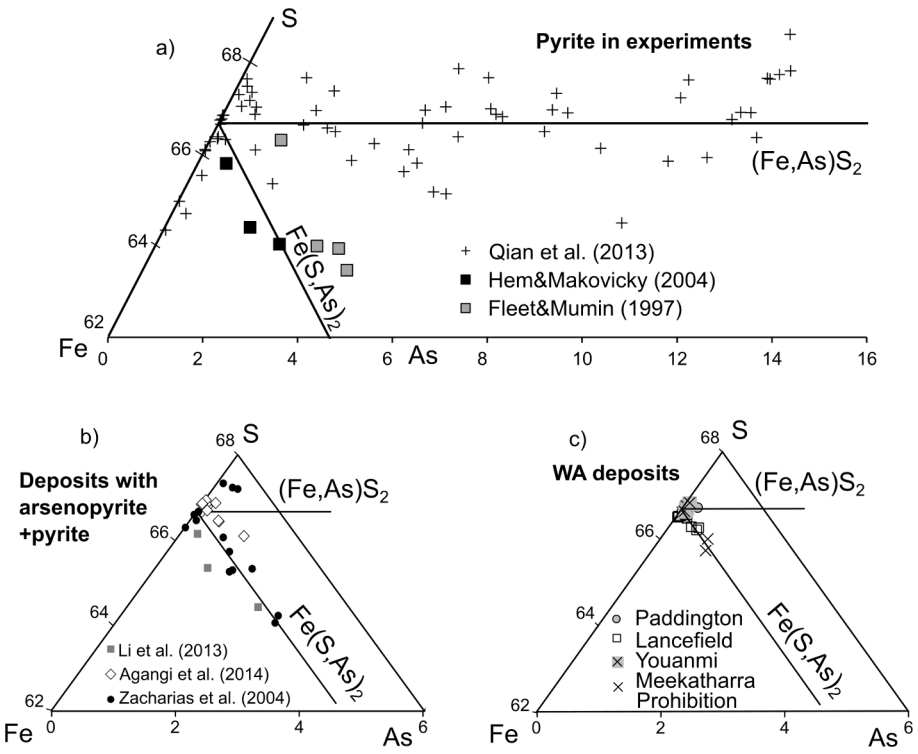

Fig. 3. Arsenic substitution types in pyrite. (a) Pyrite from experimental studies that shows both (Fe, As)S_2 and Fe(S, As)$_2$ type substitution mechanisms; (b) pyrite from the ores with pyrite and arsenopyrite assemblage that exclusively show Fe(S, As)$_2$ substitution mechanism though significant data scutter is apparent; (c) the analyses of pyrite from Western Australian deposits with pyrite and arsenopyrite assemblage showing a tight trend consistent with Fe(S, As)$_2$ mechanism.

contrary, in Meekatharra Prohibition arsenopyrite inclusions are associated with pyrite with very low As content (Fig. 4a). Moreover the textures of replacement of arsenian pyrite by aggregates of pyrite and arsenopyrite have been reported at Bogosu-Prestea mining district of the Ashanti Gold Belt, Ghana (Mumin et al., 1994), Sunrise Dam in WA (Sung et al., 2009), and Zhuangzi deposit in China (Li et al., 2018).

The textures of pyrite and arsenopyrite from sulphide deposits of Western Australia provide additional evidence against scenario A (Fig. 4). For example, pyrite from Paddington deposit shows zonation from the very low As content in core, to mantle of arsenian pyrite with highest As (1.3–1.5 wt% As) and then to rim with approximately 0.2 wt % As. The core could be interpreted as formed before the introduction of high-As fluid to the system but the mantle or rim likely formed together with arsenopyrite and no zone recorded the values of 5–6 wt% As predicted by the models (e. g. Xing et al., 2019a, 2019b). In many deposits with the pyrite and arsenopyrite assemblage, all analysed pyrites had As contents significantly lower than 6 wt% (Fig. 1b), for example 50% of deposits in Table 2 have all reported As concentrations <3 wt% As and all analyses from 4 deposits from Western Australia are <1.6 wt% (Fig. 4). The only way to reconcile such assemblages with the phase diagram of Xing et al. (2019a), Xing et al. (2019b) is to assume the complete absence of equilibrium in these occurrences, hence rendering the diagram inapplicable to the natural systems.

4.2. Scenario B: Thermodynamic control on equilibrium As content in pyrite

The critical question for this scenario of the thermodynamic control of equilibrium As solubility in arsenian pyrite (Fig. 6b) is in the specific parameters that affect the stability of arsenian pyrite in nature. In general, the main parameters that could affect the behaviour of a thermodynamic system include temperature, pressure, the activities of components, the presence of fluid and fluid composition parameters such as pH and redox conditions. Additional factors, such as mineral grain size and substitution mechanism also could play a role. To account for the effect of each thermodynamic parameter, experimental studies are required that investigate one parameter at a time and thoroughly demonstrate equilibrium between pyrite and arsenopyrite. Unfortunately, to the authors' knowledge, such data do not exist at the time of writing. The lack of equilibrium experimental data is exacerbated by lack of well documented examples of assemblages of arsenian pyrite and arsenopyrite that can be demonstrated to represent equilibrium assemblages. Nevertheless, in the discussion below, we will attempt to summarise the results of basic thermodynamic considerations with the observations from this contribution and the studies available in the literature to delineate some principal limitations on this scenario.

4.2.1. The effect of temperature and pressure

Temperature has the strongest effect on solubility and stability of components. Compounds with limited mutual solubility form a bell-shaped solvus with decreasing solubility at lower temperatures (Massalski, 1989). The compilations of As content in pyrite coexisting with arsenopyrite (Fig. 1b) and arsenian pyrite (Fig. 1c) show a conspicuous pattern of increasing As content with decreasing temperature, opposite to what is expected from a solvus. The experimental data suggest that at 500–600 °C, arsenic solubility in pyrite is 0.5–4.7 wt% (Clark, 1960; Hem and Makovicky, 2004b), however there are no data on equilibrium As solubility in pyrite at lower temperatures. Nevertheless, since the compilation of natural pyrite-arsenopyrite pairs which formed between 200 and 300 °C have variable As content down to very low concentrations (Fig. 1b), there is no evidence that at low temperatures pyrite coexisting with arsenopyrite in equilibrium has high As content.

The effect of pressure is typically small on sulfide equilibria because they have high densities and low compressibility (Barton, 1974). Chalcophile element partitioning into sulphides is also considered relatively independent of pressure (Barton, 1974; Kiseeva and Wood, 2013; Tomkins et al., 2007), in particular at relatively small pressure intervals. The majority of deposits summarised in Table 2 formed at upper crustal

Table 2
A summary of compositions of pyrite coexisting with arsenopyrite in various deposits from a literature survey.

Locality	Type	As wt% Max–Min	Average wt%	Pyrite type coexisting with arsenopyrite	T°C	References
Paddington, WA, Australia	Orogenic (Precambrian)	0.2–0.44		Rim Py		This study, Belousov et al. (2016)
Meekatharra Prohibition, WA, Australia	Orogenic (Precambrian)	<0.03–1.6				This study, Belousov et al. (2016)
Lancefield, WA, Australia	Orogenic (Precambrian)	<0.03–0.9			280 ± 30	This study, Belousov et al. (2016), Salier et al. (2005)
Youanmi, WA, Australia	Orogenic (Precambrian)	<0.03–0.09				This study, Belousov et al. (2016)
Sheba and Fairview gold Mines, South Africa	Orogenic (Precambrian)	0.17–0.21	0.19	Py 62_11 Stage 1	300–420	Agangi et al., (2014)
Tanami gold province, NT, Australia	Orogenic (Precambrian)	0.2–0.4				Cook et al. (2013)
Babaikundi area, India	Orogenic (Precambrian)	0.01–1.85				Jha et al. (2015)
Pampe deposit, Ghana	Orogenic (Precambrian)	0.09–0.65		Py from V2 vein set		Salvi et al. (2016)
Sunrise Dam, WA, Australia	Orogenic (Precambrian)	0.02–5.7			280–320	Sung et al. (2009), Salier et al. (2005)
Daqiao deposit, China	Orogenic	0.01–0.8		Py4-py		Wu et al. (2019a), Wu et al. (2019b)
Zhengchong, China	Orogenic	1–4.2		PyII-1, PyII-2		Shao et al. (2018)
Yangshan gold belt, Qinling, China	Orogenic/epizonal Orogenic/epizonal	0.68–10.7 0.02–3.59		Py2 main ore stage Py3 late ore stage		Li et al., (2014)
Buracão Area, Brazil	Orogenic	0.16–1.11		Py from veins	260–450	Pires et al., (2019)
Bake deposit, China	Orogenic	0.02–1		P0		Liu et al. (2018)
Um Garayat deposit, Egypt	Orogenic	0.08–0.36		Blocky pyrite	340–360	Zoheir et al. (2019)
Gutaishan deposit, China	Orogenic	0.16–1.9		Py2a,2b,3a		Li et al. (2019)
Suzdal, Kazakhstan	Orogenic	0.2–4.31			300–380	Kovalev et al. (2011), Kovalev et al. (2009)
Maureen deposit Queensland, Australia	Orogenic	2.3–7.7	4.9		250–300	Hurtig et al. (2014)
Sawayaerdun, Xinjiang, China	Orogenic	0.03–8	1.74	Py1 and Py2	220–270	Zhang et al. (2017)
Wangu gold deposit, Hunan, China	Orogenic/ intracontinental reactivation	2.0–5.93	3.3		245–387	Deng et al. (2017)
Bhukia-Jagpura gold prospect, India	Metamorphosed orogenic?	0.014–0.021		Py IV with Po	Peak 530–550	Deol et al. (2012)
Homestake, USA	Orogenic (metamorphosed)	0.001–0.3		Py2	500°±50	Steadman and Large (2016)
Rosebery Deposit, Tasmania, Australia	VMS	0.04–0.58	0.18		250–300	Smith and Huston (1992)
Kuh-Pang deposit, Iran	VMS	0.01–4.18	1.76		250–370	Rajabpour et al. (2017)
Brunswick No. 12 deposit, Canada	VMS	0.02–1.05	0.21		350–450 °C	McClenaghan et al. (2009)
Ming Mine, Newfoundland, Canada	VMS	1.07–8.24	2.9	Up Plunge Pyrite	250–300	Brueckner et al. (2014)
Chouichia and Ain el Bey, Tunisia	Epithermal?	2.5–9.3	5.0	Py Stage 2	200–300	Slim-Shimi et al. (1996)
Vorontsovskoe, Urals, Russia	Epithermal/skarn	0.09–0.36	0.22	A3 type Py	310–400	Murzin et al. (2017)
Patricia deposit, Chile	Epithermal	0.83 – 2.7 0.12–1.85	1.76	Pre-ore (Py1) Post-ore (Py3)	210–250 180–240	Chinchilla et al. (2016)
Huijiabao Trend, China	Carlin	0.48–9.83	4.2	Py3, Py4	210 ± 20	Hou et al. (2016)
West Banshee, USA	Carlin		3.0	Stage 3		Barker et al. (2009)
Jinlongshan, China	Carlin	<0.02–7.27		Py1–Py2		Zhang et al. (2014)
Zhuangzi deposit, China	Unclear	0.17–3.92 <0.02–0.2	1.8 0.1	Py1 Py2	289–375 289–375	Li et al. (2018)
Gutaishan, China	Unclear	0.03–1.93 0.12–1.85	0.6 0.98	Py2 Py3	200–320 175–215	Li et al. (2019)
Lianhuashan ore field, China	Unclear	0.001–6.5	1	Py2	~ 200	Hu et al. (2018)
Marche-Combrailles Shear Zone, France	Unclear	2–4	3.25	Pyrite IV	240 ± 30	Boiron et al. (1989)
Roudny deposit, Bohemian Massif, Czech Republic	Unclear	0.02–4.66		pyrite-2		Zacharias et al. (2004)
Zaozigou deposit, China	Unclear	0.5–4	2.2		148–304	Tang et al. (2019)
El Sid Gold Mine, Egypt	Unclear	0.072 – 0.2	0.072			El-Bouseily et al. (1985)

conditions at relatively low-pressure and a major role for pressure in stabilisation of arsenian pyrite is unlikely.

4.2.2. *The effect of grain size*

Grain size could be another parameter affecting the stability of pyrite and As content. Fine-grained aggregates have higher total energy than coarse-grained crystals due to a contribution of surface energy. Arsenian pyrite could occur both in fine-grained aggregates and as coarse crystals (Fig. 5). Deditius et al. (2008) observed that arsenian pyrite forming micro-size grains (<1 μm) is composed of nanoparticulate aggregates of single crystals of arsenian pyrite and reported an increase of As content in smaller nanocrystals of pyrite with (Fe, As)S_2 substitution from Yanacocha deposit. A correlation with highest Au concentrations (up to about 900 ppm Au) in aggregates of smallest pyrite grains was observed by Simon et al. (1999a), Simon et al. (1999b) in a Carlin-type deposit. Qian et al. (2013) synthesised texturally similar nano-crystalline pyrite in experiments on replacement of magnetite. In contrast, euhedral pyrite produced by the hydrothermal replacement of carbonates, had higher As content than fine-grained framboidal and porous pyrite (Kusebauch et al., 2018b). Overall, while the grain size commonly shows correlations with pyrite composition in many environments, it does not seem to be the primary factor controlling As content, since both coarse crystalline pyrite and fine-grained pyrite with high As concentrations are commonly observed (Deditius et al., 2008; Peterson and Mavrogenes,

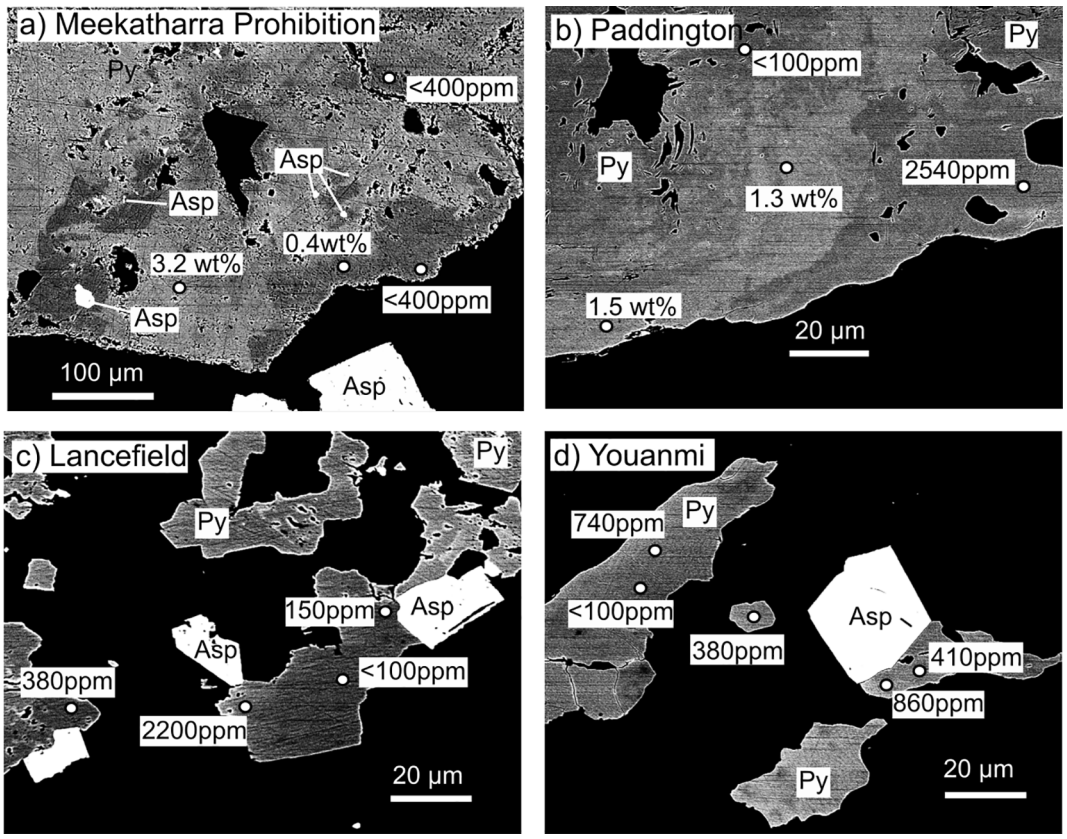

Fig. 4. BSE images of pyrite from deposits in Western Australia with assemblage of pyrite and arsenopyrite with As concentration in representative zones of pyrite obtained by EPMA. The image collection was optimized for visualisation of pyrite zonation and the matrix assemblages of silicates and carbonates are not resolved in the black background of the images due to low BSE signal of these minerals. Brightness of pyrite grains reflects variations in As content. Note low concentrations of As in pyrite coexisting with arsenopyrite and at distances of 10 s to100s micron.

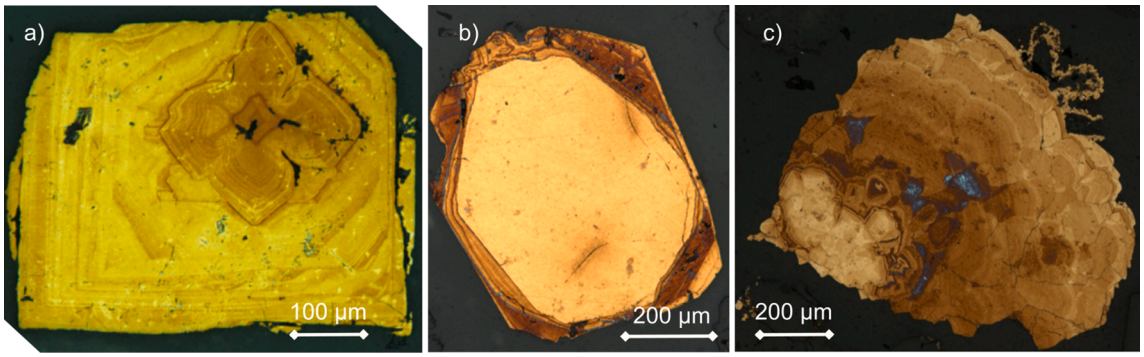

Fig. 5. Reflected light images of sector and oscillatory zoning in pyrite from Lihir gold deposit, Papua New Guinea etched with NaClO. The details on the deposit are provided in Sykora et al. (2018) and etching technique was described by Peterson and Mavrogenes (2014). The bands of darker brown colour correspond to higher As content in pyrite (Peterson and Mavrogenes 2014). The sector and oscillatory zoning visible in Lihir pyrite are typical products of surface-controlled disequilibrium growth (Watson, 1996). a) A pyrite crystal with intense sector and oscillatory zoning that shows transition from original octahedral morphology to cubic crystal shape. b) A pyrite crystal with large euhedral core composed of pyrite low trace element content and without, visible zonation, surrounded by a rim with fine oscillatory zoning and sector zoning; c) a polycrystalline, possibly botryoidal aggregate of pyrite with oscillatory zoning.

2014; Sykora et al., 2018).

4.2.3. The effect of the activity of components

The stability and composition of arsenian pyrite as a phase in the Fe-As-S system can be affected by the activities of the components such as As and S (aS_2 for sulfur activity and aAs for As activity). The effect of the activity of the components on the stability of phases in the system Fe-As-S was evaluated by Barton (1969) who demonstrated that at constant P and T, the phase rule predicted that the assemblage of pyrite with arsenopyrite occurs on a line in aS_2–aAs space. The assemblages of the three phases define nonvariant points, and the line of coexisting pyrite and arsenopyrite is limited by the point pyrite coexisting with arsenopyrite and pyrrhotite at lower S and As activity, and pyrite and arsenopyrite coexisting with sulfur-arsenic liquidat higher S and As activity (Fig. 7). When pyrite is in equilibrium with arsenopyrite, then the activity of arsenic is proportional to the activity of sulfur (Fig. 7b). The composition of pyrite in the buffered assemblage of mss/pyrrhotite, pyrite and arsenopyrite in the system containing Co and Ni was reported

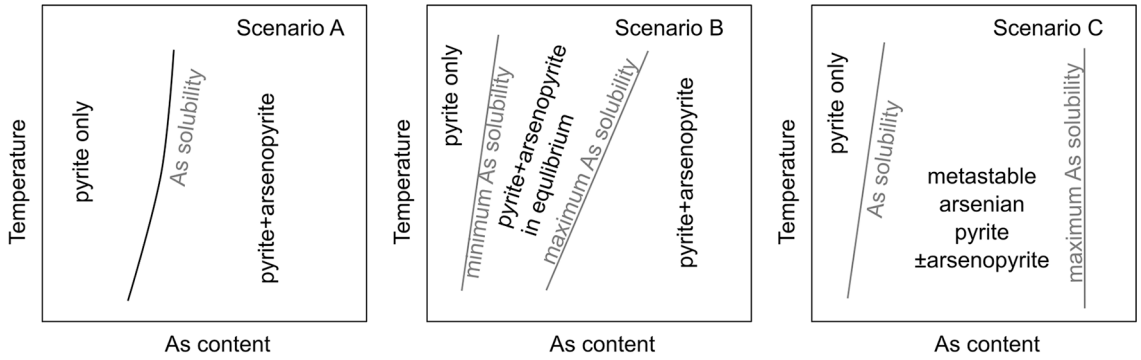

Fig. 6. A schematic plot of principal scenarios of the phase relation between arsenian pyrite and arsenopyrite. See discussion in the text.

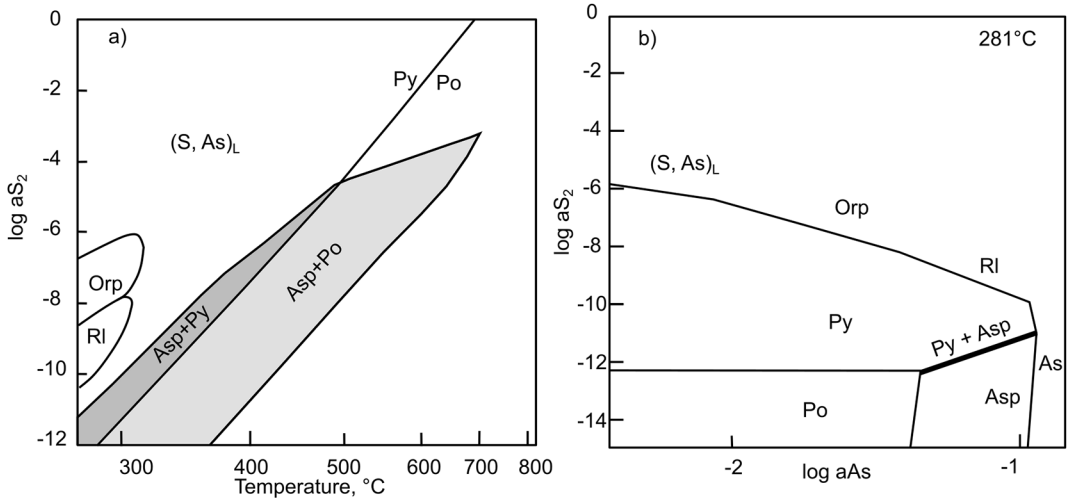

Fig. 7. a) Simplified sulfur activity ($aS2$) versus temperature diagram (Kretschmar and Scott, 1976; Tomkins et al., 2006) that shows the fields of the coexisting pyrite and arsenopyrite and pyrrhotite and arsenopyrite. b) Sulfur activity versus arsenic activity (aAs) diagrams relevant for stability of arsenopyrite and pyrite (Barton, 1969). The thickened line shows coexistence of pyrite with arsenopyrite. Abbreviations are the same as in Fig. 2.

by Hem and Makovicky (2004a), however, no experimental or natural data are available on the composition of pyrite in equilibrium assemblages with higher aS_2/aAs such as assemblages with sulfur-arsenic liquid. Considering that pyrite with arsenopyrite is stable over less than one order of magnitude of S and As activity at any given temperature (Fig. 7), it is unlikely that the increase of S and As activities alone could control the composition of pyrite with As concentration varying by over three orders of magnitude.

4.2.4. The effect of the fluid composition

The composition of fluids can have a profound effect on the solubility of minerals and hence control their transporting ability. The effects of the pH and H_2S activity on the solubility of arsenopyrite in a fluid have been studied by experiments where the attainment of equilibrium has been demonstrated by saturation and dissolution experiments (Perfetti et al., 2008; Pokrovski et al., 2002). Among the experiments on arsenian pyrite available so far, those that attempted to achieve equilibrium have been performed only in dry systems. The fluid-bearing experiments of Fleet and Mumin, (1997) produced arsenian pyrite that was interpreted as a metastable product in addition to the observed metastable arsenian marcasite. Other hydrothermal experiments produced highly zoned, often fine-grained pyrite aggregates that also likely represent metastable products where composition was controlled by the reaction path (Kusebauch et al., 2018a; Qian et al., 2013). In the absence the equilibrium hydrothermal experiments with arsenian pyrite we consider the natural samples observations and the thermodynamic constraints on the system.

Stepanov (2019) criticised the model by Xing et al. (2019a), Xing et al. (2019b) because it failed to reproduce some of the key experimental observations of the system. One such disagreement is that maximum temperature of stability of the assemblage of pyrite and arsenopyrite is 491 °C (Fig. 2 and Fig. 7) (Kretschmar and Scott, 1976) and slightly above 500 °C according (Hem and Makovicky, 2004a). The temperature increases by 14 °C per kbar with pressure (Sharp et al., 1985). The calculations of Xing et al. (2019a) estimated the highest temperature of the assemblage pyrite-arsenopyrite was at about 580 °C and 2 kbar, about 60 °C higher than estimates from experiments. Xing et al. (2019b) explained this discrepancy by the dissolution of significant amounts of Fe and S by the hydrous fluid. They proposed that the limits of thermal stability of assemblages of arsenopyrite and pyrite established in dry systems did not apply to water-bearing systems. However, since all minerals in Fe-As-S system are anhydrous, the presence of H_2O cannot have a direct effect on the stability and composition of the minerals. When additional components are present in the system, then the stability field of some minerals could diminish due to their solubility in the fluid. For example, As-S melt/liquid that is present in the dry Fe-As-S system is unlikely to occur in hydrous systems. However, the presence of water in the system cannot increase the maximum stability temperature of an assemblage of anhydrous minerals such as pyrite and arsenopyrite (Barton, 1974; Tomkins et al., 2007).

The role of a fluid in mineral–mineral equilibria can be demonstrated on the simpler phase relations of pyrite and pyrrhotite. Pyrrhotite has a

variable composition $Fe_{(1-x)}S$ depending on temperature and fS_2 (Toulmin and Barton, 1964). The composition of pyrrhotite coexisting with pyrite at any given temperature and pressure is independent of the presence of fluid and fluid composition (Kishima, 1989; line of coexisting pyrite and pyrrhotite at Fig. 7a). Similarly, the effect of fluid composition on composition of pyrite in equilibrium with arsenopyrite could be only indirect, for example, by affecting the activity of S/As in the system. Notwithstanding the arguments presented above, the effect of fluid on the phase relations between pyrite and arsenopyrite requires further studies at clearly defined equilibrium and disequilibrium conditions.

4.2.5. *The effect of redox conditions and As substitution mechanism*

Redox state is an essential parameter during crystallisation of As-bearing pyrite because As occurring as $As^{+3}(OH)_3$ in solutions (Perfetti et al., 2008; Pokrovski et al., 1996) changes to As^{-1} or As^{+2} in pyrite depending on the mechanism of As substitution in pyrite (Qian et al., 2013). Of the two main substitution types, the $Fe(S,As)_2$ substitution is by far the most common in pyrite coexisting with arsenopyrite in hydrothermal ore deposits (Section 2.3, Fig. 3). Because in pyrite with Fe $(S,As)_2$ substitution As is in the same state As^{-1} as in arsenopyrite Fe(S, $As)_2$ the exchange of As between minerals can occur without redox reactions and hence the As content in $Fe(S,As)_2$ pyrite could be independent of the redox conditions. This point was inadvertently illustrated by the model of Xing et al. (2019a) that showed that at oxidised and reduced conditions the As content of pyrite coexisting with arsenopyrite remained the same. For example, they estimated that irrespective of redox conditions at approximately 180 °C, the As content in pyrite coexisting with arsenopyrite is 5 wt% (yellow vertical lines in the field of pyrite and arsenopyrite at Fig. 2C and D in Xing et al. (2019a)). While the exact values of As concentrations are in disagreement with the experimental and natural data (Fig. 1), the modelling by (Xing et al., 2019a) suggests that redox conditions have no effect on As solubility in pyrite with $Fe(S,As)_2$ type substitution.

The pyrite with $(Fe,As)S_2$ substitution has been observed in Yanacocha deposit (Deditius et al., 2008) and was synthesised in experiments by Qian et al. (2013). In Yanacocha deposit $(Fe,As)S_2$ pyrite formed under rapid local changes in temperature and/or the chemical composition of the mineralising fluids at non-equilibrium conditions (Deditius et al., 2008). The wide range of As contents, intensive zonation and the fine-grained textures suggest that this type also formed by disequilibrium crystallisation. As there is no evidence of equilibrium in assemblages with this type of pyrite, probably the pyrite with $(Fe,As)S_2$ substitution is always a product of reaction path dependent disequilibrium crystallisation (Qian et al., 2013; Xing et al., 2019a).

4.3. *Scenario C: Metastability of arsenian pyrite*

The growth of a mineral from a hydrothermal solution occurs by the absorption of atoms to the surface of the crystal. It commonly results in disequilibrium compositions of minerals because the energy of atoms in the crystal volume (that define the energy of a thermodynamic substance) is generally different from the energy of atoms on the surface of a crystal (Watson, 1996): "…*crystal is growing, any trace elements bound in the surface layer may be buried and trapped in the newly-formed lattice, resulting in lattice concentrations that deviate substantially from those predicted by equilibrium partitioning between the crystal and its growth medium*". The disequilibrium composition of the surface followed by burial by the new layers and then intracrystalline diffusion is necessary for homogenisation of the mineral composition and equilibration with the fluid and surrounding crystals. Therefore, the phenomena controlling the mineral growth in the fluid (diffusion in fluid, development of the boundary layer), on the surface (nucleation and adsorption) and inside the crystal (intracrystalline diffusion or lack of thereof) can lead to deviations of the mineral composition from equilibrium.

As the models of equilibrium relations between arsenian pyrite and arsenopyrite cannot describe the observed phase relations, there is a need for an additional mechanism. One of the possible explanations is metastability, i.e. the existence of phases stable outside the conditions of thermodynamic stability or phases without stability fields (Brazhkin, 2006a, 2006b). Metastable phases are commonly described in chemistry and metallurgy. In fact, the majority of organic compounds and useful alloys are metastable relative to simpler and more thermodynamically stable compounds (Turnbull, 1981; Brazhkin, 2006a, 2006b). Metastability is also widespread in the mineral world (e. g. Korsakov et al., 2010; Starr and Pattison, 2019). The interpretation that arsenian pyrite could be a metastable/disequilibrium phase has been proposed in several studies (Ballantyne and Moore, 1988; Fleet et al., 1993; Fleet and Mumin, 1997; Reich and Becker, 2006; Sykora et al., 2018), though was not favoured by recent models (Xing et al., 2019b). Scenario C of widespread metastability/disequilibrium between arsenian pyrite and arsenopyrite (Fig. 7) could offer solutions to some conundrums of the system but also triggers new questions.

4.3.1. *The role of surface processes in crystallisation of arsenian pyrite*

The characteristic features of absorption-controlled growth are sector and oscillatory zoning (Reeder and Paquette, 1989; Shtukenberg et al., 2009; Watson, 1996), which are common in pyrite (Chouinard et al., 2005; Fleet et al., 1988; Peterson and Mavrogenes, 2014; Sykora et al., 2018). Sector zoning (Fig. 5) is a specific indicator of disequilibrium partitioning during growth because it could only develop when growth of different facies produces different mineral compositions, whereas the equilibrium growth of the mineral should result in a homogeneous composition (Watson, 1996). Oscillatory zoning could form due to different processes, which include changes in the chemistry of fluids, variations in growth rate and growth controlled by the diffusion from the solution and commonly indicates disequilibrium crystallisation processes (Tiller and Ahn, 1980; Watson, 1996). Therefore, the common presence of intense zonation in arsenian pyrite is an evidence for the disequilibrium conditions during crystallization of arsenian pyrite.

Gold is an important impurity in pyrite commonly correlating with As contents in the mineral (Deditius et al., 2014; Kusebauch et al., 2019; Large and Maslennikov, 2020; Reich et al., 2005; Simon et al., 1999a). In the low-As systems pyrite can have relatively low partitioning coefficients for Au (Pokrovski et al., 2019) and can be associated with Te (Large and Maslennikov, 2020). The processes proposed as responsible for high contents of gold in arsenian pyrite include:

- chemisorption (Fleet and Mumin, 1997);
- localisation of highly reducing conditions at the surface of arsenic-rich minerals during dissolution (Pokrovski et al., 2019, 2002);
- electrochemical accumulation of gold on charged p-type pyrite surfaces (Möller and Kersten, 1994);
- formation of particles which are stable only on a pyrite substrate (non-autonomous nano-particles; Tauson et al., 2014, 2010);
- coupled As-Au partitioning into pyrite in As-bearing systems (Kusebauch et al., 2019) and chemisorption in As-free systems (Pokrovski et al., 2019).

The majority of these mechanisms emphasise the important role of adsorption in the formation of high-Au and high-As pyrite and these processes inherently tend to result in the heterogeneous composition of the mineral unless it is homogenised by diffusion (Watson, 2004). High concentrations of Au are typically observed in pyrite with As content above 1 wt% As (Reich et al., 2005), that falls in the range of metastable pyrite compositions proposed in this study (Fig. 8). Therefore, the future studies investigating the mechanisms of Au concentration in pyrite should investigate the role of metastability in pyrite-arsenopyrite system.

4.3.2. *The role of solid state diffusion in pyrite*

After entrapment, the composition of a mineral that is in equilibrium

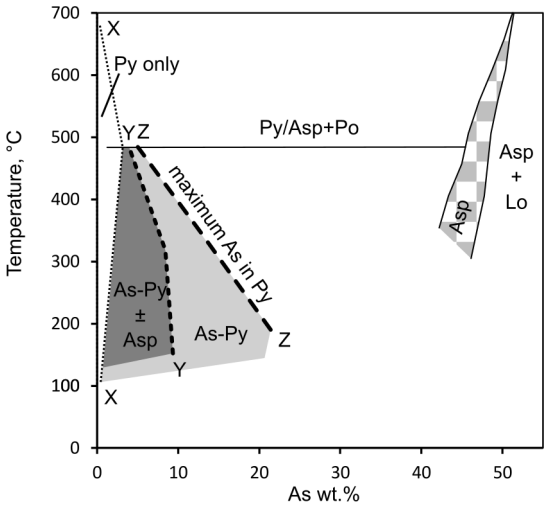

Fig. 8. A subset of the FeS_2–$FeAs_2$ phase diagram with the fields of pyrite composition delineated based on the data from Fig. 1. The compositional range of arsenopyrite is shown after Kretschmar and Scott (1976). The line X–X represents potential solubility of As in pyrite in equilibrium with arsenopyrite, line Y–Y shows maximum As content in pyrite coexisting with arsenopyrite and Z–Z is maximum As in arsenian pyrite.

with surrounding phases can be achieved by solid state diffusional exchange and recrystallisation. Therefore, intracrystalline diffusion in pyrite and arsenopyrite are the principal parameters that govern the attainment of equilibrium between the minerals in nature and experiments. Unfortunately, there are no estimates of the diffusion rates in arsenopyrite and information on diffusion rates in pyrite is very limited: Brenan et al., (2000) measured the diffusion of Os and Watson et al. (2009) estimated the diffusion rate of sulfur isotopes. All available experimental estimates suggest extremely slow diffusion in pyrite. Additional constraints on the diffusion rate in pyrite are the observations that pyrite in natural rocks typically has strong and sharp compositional zonation (Figs. 4, 5) also suggesting very slow diffusion rates in the mineral (Peterson and Mavrogenes, 2014; Sykora et al., 2018).

The common preservation of the growth zonation in pyrite coupled with the very slow diffusion suggests that arsenian pyrite could be considered as a metastable phase, defined as "*…a nonequilibrium state of a substance whose properties change reversibly over a period of the experiment or observation*" (Brazhkin, 2006a, 2006b). Low diffusion rate prevents the mineral from homogenization that is necessary for achieving equilibrium composition.

4.3.3. The effect of temperature on the crystallisation of arsenian pyrite

Temperature affects the disequilibrium uptake of trace elements in multiple ways (Watson, 2004, 1996). The increase of temperature increases diffusion in the growth medium (fluid) and hence decreases the development of the boundary layer during crystal growth. Temperature also increases the rate of intracrystalline diffusion in the mineral and hence can facilitate the attainment of equilibrium. The negative slope of maximum As concentrations with temperature (Figs. 1 and 8) is in agreement with the model of Watson (1996) that proposed that with an increase in temperature, the efficiency of entrapment of trace elements decreases. However, the relative role of the increase of diffusion in the fluid and the crystal and changes in fluid composition with the temperature needs to be established by further studies.

The rate of mineral growth could be another important parameter likely affecting the incorporation of impurities, such as As into pyrite. It has been proposed that a lower rate of mineral growth can result in crystallisation of pyrite with lower contents of trace elements other than Ni, Co, Se, and Te that are isomorphic with either Fe or S (Abraitis et al., 2004; Sykora et al., 2018). High growth rate results in disequilibrium adsorption of atoms to the mineral surface and also covering by the new layers, hence preventing from reaching equilibrium. In the case study of Lihir gold deposit, PNG Sykora et al. (2018) proposed that at the high temperature of porphyry stage, growth rate was lower resulting in the low content of trace elements, whereas at the low temperatures of the epithermal stage the growth rate was higher producing pyrite with high contents of trace elements including As. The crystal growth rate is closely related to the fluid (over-) saturation and cooling rate that likely were different between the two stages of ore genesis in Lihir deposit. Overall, with decreasing temperature there is a multitude of factors that favour the development of surface-controlled crystal growth that results in crystallization of arsenian pyrite.

4.3.4. The effect of fluid composition on surface-controlled pyrite crystallisation

The scenario of metastable crystallisation of arsenian pyrite does not exclude the effect of the thermodynamic parameters such as fluid composition on pyrite crystallisation as it could play an essential role during disequilibrium crystallisation as well. Pyrite growth from oversaturated solutions, commonly occurs by the reaction of S-rich fluid with Fe bearing minerals (Fleet and Mumin, 1997; Kusebauch et al., 2018b; Qian et al., 2013). In natural fluids at equilibrium, arsenic mainly occurs as $As(OH)_3$ (Perfetti et al., 2008; Pokrovski et al., 1996, 2002). Hydrothermal replacement experiments (Kusebauch et al., 2018b) demonstrated that As partitioning coefficients between pyrite and fluid decrease with As content in the fluid, whereas equilibrium partitioning is expected to be independent of the concentration (e. g. Barton, 1974). The experiments by Qian et al. (2013) demonstrated that fluids that sourced As from such minerals as arsenopyrite and lollingite precipitated pyrite with considerably lower As content (maximum 0.6 wt% As) than pyrite formed from the fluids that dissolved As from such substances as As_2O_3 (up to 23.8 wt% As as (Fe, As)S_2 solid solution). This evidence of the dependence of pyrite composition from As sources might suggest that sorption properties of pyrite could be different in fluids with different compositions, however further studies are needed to understand the relative role of equilibrium and the disequilibrium processes and different fluid compositional parameters on the composition of arsenian pyrite.

5. Implications

In this contribution we suggest that high-As pyrite could be a metastable phase at much lower As concentrations than previously thought. The potential metastability of high-As pyrite has significant implications for the interpretation of this mineral's behaviour during metamorphism of sediments and ore deposits. Pyrite is the major host of chalcophile elements in sediments and low grade metamorphic rocks (Gregory et al., 2015). Fluids forming orogenic gold deposits are produced by the dehydration of sediments during metamorphism (Evans et al., 2006; Phillips and Powell, 2010; Stepanov, 2021; Tomkins, 2010), and the most likely source of Au and As in fluids is sedimentary pyrite in black shales (Pitcairn et al., 2006, 2010, 2014; Large et al., 2007, 2012, 2011; Tomkins, 2010; Thomas et al., 2011). The decomposition of pyrite to pyrrhotite was proposed as the main mechanism controlling the release of Au and As to the metamorphic fluid(s) (Pitcairn et al., 2010; Large et al., 2011; Thomas et al., 2011). The recrystallization of high-As and high-Au sedimentary pyrite during the metamorphic devolatilization can be one of the mechanisms of generation of Au-rich fluids during low grade metamorphism. The recrystallization of metastable arsenian pyrite could explain the survival of metamorphic pyrite to higher temperature conditions than the "window" of generation of Au-bearing fluids that is observed in some zoned metamorphic complexes (Ferry, 1981; Pitcairn et al., 2015).

The metastability of high-As pyrite has implications for interpretation of sulfide assemblages. The geothermometry of sulfide assemblages is known to be problematic, especially for pyrite (Barton, 1974). To date

there is no reliable method to determine the temperature of pyrite formation from its composition, although attempts have been made to use the partitioning of sulfur isotopes between individual growth sectors of pyrite (van Hinsberg et al., 2010). Also, many sulfide minerals show little variation in partitioning of trace elements with temperature (George et al., 2016). The metastability of arsenian pyrite might offer an explanation for the consistent difficulty in development of reliable geothermometers for pyrite.

The pyrite geochemistry has been used for numerous geochemical problems, including the use of the systematic variations in Au concentrations in sedimentary pyrite for estimation of Au content in ocean water though time (Large et al., 2015a), tracing of biologically important nutrient elements during history of the ocean (Large et al., 2015b), the usage of geochemistry of pyrite as a pathfinder for ore mineralisation (Large et al., 2017); and as a recorder of the geochemistry of ore-forming fluids (Tardani et al., 2017). These applications do not require the equilibrium partitioning of trace elements between pyrite and fluid. As long as pyrite preserves composition from the growth event and provided that suitable partition coefficients have been estimated, the compositions of pyrite can be a sensitive indicator of the composition of the solutions that produced this mineral.

6. Conclusions

In this study, we have reviewed the compositions of experimentally produced and naturally coexisting pyrite and arsenopyrite and elaborate on the phase relations of arsenian pyrite and arsenopyrite. While our study highlights the need for new experimental and theoretical data on the system, the following observations are pertinent from this review:

- The experimental studies that attempted to achieve equilibrium synthesised pyrite containing from <1 to 4.7 wt% As.
- The published data from natural samples demonstrate highly heterogenous pyrite in terms of As concentrations and the widespread occurrence of low-As (e. g. <3 wt% As) pyrite coexisting with arsenopyrite.
- In assemblages without arsenopyrite, the As content in pyrite can attain higher concentrations than in arsenopyrite-bearing assemblages.
- We discussed three possible scenarios that could potentially explain the conundrums of the system, including (A) equilibrium crystallisation between only high-As pyrite (5–6 wt% As) and arsenopyrite; (B) strong dependence of As content in pyrite on thermodynamic parameters (e. g. temperature, fluid presence and composition) and (C) equilibrium of low-As pyrite (<1 wt% As) with arsenopyrite and metastable crystallisation of arsenian pyrite.
- Scenario A of stable coexistence of arsenian pyrite and arsenopyrite fails to explain multiple observations in natural samples.
- Scenario B of the considerable variation of pyrite composition in equilibrium with arsenopyrite is constrained by the limits of the stability of the assemblage of pyrite and arsenopyrite.
- Scenario C of the metastability of arsenian pyrite allows explanation of multiple observations including the widespread heterogeneity of arsenian pyrite, textures of decomposition and the surface control on mineral chemistry.
- The highest As content in arsenian pyrite is found in arsenopyrite-free environments in Carlin-type deposits.
- Experimental constraints such as As partitioning coefficients between pyrite and fluid estimated by Kusebauch et al. (2018) and arsenopyrite solubility (Perfetti et al., 2008; Pokrovski et al., 2002) are independent of the interpretations of the phase relation of arsenian pyrite and arsenopyrite, however, the possibility of the extensive metastability should be considered in the planning of the future experimental studies as was done by Pokrovski et al. (2002).
- This study represents a reconnaissance attempt of delineation of metastability in the system pyrite-arsenopyrite. A number of recent studies investigated the crystallisation at conditions typical for hydrothermal ore deposits, however, experimental data in the high-temperature range of conditions are limited: the principal study by Clark (1960) was conducted almost 60 years ago and since has not been reproduced. Additional experimental and natural studies will be required to obtain better constraints on phase relations in the critically important systems involving pyrite and arsenopyrite.

Declaration of Competing Interest

The authors declare that they have no known competing financial interests or personal relationships that could have appeared to influence the work reported in this paper.

Acknowledgements

We thank the Geological Survey of Western Australia for providing samples used in this study. Vadim Brazhkin provided valuable insights into the definition and thermodynamics of metastable phases. Two anonymous reviewers are thanked for constructive reviews, and Arthur Deditius, Christof Kusebauch and Gleb Pokrovski are acknowledged for insightful discussions. This study was supported by the National Natural Science Foundation of China (No. 42073058 and No. 42073036). The work of Kate Kiseeva in Oxford University was financially supported by NERC grant NE/L010828/1.

Appendix A. Supplementary data

Supplementary data to this article can be found online at https://doi.org/10.1016/j.oregeorev.2021.104285.

References

Abraitis, P.K., Pattrick, R.A.D., Vaughan, D.J., 2004. Variations in the compositional, textural and electrical properties of natural pyrite: a review. International Journal of Mineral Processing 74, 41–59. https://doi.org/10.1016/j.minpro.2003.09.002.

Agangi, A., Hofmann, A., Przybyłowicz, W., 2014. Trace element zoning of sulfides and quartz at Sheba and Fairview gold mines: Clues to Mesoarchean mineralisation in the Barberton Greenstone Belt, South Africa. Ore Geology Reviews 56, 94–114. https://doi.org/10.1016/j.oregeorev.2013.08.016.

Ballantyne, J.M., Moore, J.N., 1988. Arsenic geochemistry in geothermal systems. Geochimica et Cosmochimica Acta 52, 475–483. https://doi.org/10.1016/0016-7037(88)90102-0.

Barton, P.B., 1974. Sulfide petrology. Sulfide Mineralogy, Reviews In Mineralogy. 187–198.

Barker, S.L.L., Hickey, K.A., Cline, J.S., Dipple, G.M., Kilburn, M.R., Vaughan, J.R., Longo, A.A., 2009. Uncloaking Invisible Gold: Use Of Nanosims To Evaluate Gold, Trace Elements, And Sulfur Isotopes In Pyrite From Carlin-Type Gold Deposits. Economic Geology 104, 897–904. https://doi.org/10.2113/econgeo.104.7.897.

Barton, P.B., 1969. Thermochemical study of the system Fe-As-S. Geochimica et Cosmochimica Acta 33, 841–857. https://doi.org/10.1016/0016-7037(69)90031-3.

Belousov, I., Large, R.R., Meffre, S., Danyushevsky, L.V., Steadman, J., Beardsmore, T., 2016. Pyrite compositions from VHMS and orogenic Au deposits in the Yilgarn Craton, Western Australia: Implications for gold and copper exploration. Ore Geology Reviews 79, 474–499. https://doi.org/10.1016/j.oregeorev.2016.04.020.

Blanchard, M., Alfredsson, M., Brodholt, J., Wright, K., Catlow, C.R.A., 2007. Arsenic incorporation into FeS2 pyrite and its influence on dissolution: A DFT study. Geochimica et Cosmochimica Acta 71, 624–630. https://doi.org/10.1016/j.gca.2006.09.021.

Boiron, M.-C., Cathelineau, M., Trescases, J.-J., 1989. Conditions of gold-bearing arsenopyrite crystallization in the Villeranges Basin, Marche-Combrailles shear zone, France; a mineralogical and fluid inclusion study. Economic Geology 84, 1340–1362. https://doi.org/10.2113/gsecongeo.84.5.1340.

Brazhkin, V.V., 2006a. Metastable phases, phase transformations, and phase diagrams in physics and chemistry. Phys.-Usp. 49, 719. https://doi.org/10.1070/PU2006v049n07ABEH006013.

Brazhkin, V.V., 2006b. Metastable phases and 'metastable' phase diagrams. J. Phys.: Condens. Matter 18, 9643–9650. https://doi.org/10.1088/0953-8984/18/42/010.

Brenan, J.M., Cherniak, D.J., Rose, L.A., 2000. Diffusion of osmium in pyrrhotite and pyrite: implications for closure of the Re–Os isotopic system. Earth and Planetary Science Letters 180, 399–413. https://doi.org/10.1016/S0012-821X(00)00165-5.

Brueckner, S.M., Piercey, S.J., Sylvester, P.J., Maloney, S., Pilgrim, L., 2014. Evidence for Syngenetic Precious Metal Enrichment in an Appalachian Volcanogenic Massive Sulfide System: The 1806 Zone, Ming Mine, Newfoundland, Canada. Economic Geology 109, 1611–1642. https://doi.org/10.2113/econgeo.109.6.1611.

Cafagna, F., Jugo, P.J., 2016. An experimental study on the geochemical behavior of highly siderophile elements (HSE) and metalloids (As, Se, Sb, Te, Bi) in a mss-iss-pyrite system at 650°C: A possible magmatic origin for Co-HSE-bearing pyrite and the role of metalloid-rich phases in the fractionation of HSE. Geochimica et Cosmochimica Acta 178, 233–258. https://doi.org/10.1016/j.gca.2015.12.035.

Chinchilla, D., Ortega, L., Piña, R., Merinero, R., Moncada, D., Bodnar, R.J., Quesada, C., Valverde, A., Lunar, R., 2016. The Patricia Zn–Pb–Ag epithermal ore deposit: An uncommon type of mineralization in northeastern Chile. Ore Geology Reviews 73, 104–126. https://doi.org/10.1016/j.oregeorev.2015.10.026.

Chouinard, A., Paquette, J., Williams-Jones, A.E., 2005. Crystallographic Controls On Trace-Element Incorporation In Auriferous Pyrite From The Pascua Epithermal High-Sulfidation Deposit, Chile-Argentina. The Canadian Mineralogist 43, 951–963. https://doi.org/10.2113/gscanmin.43.3.951.

Clark, L.A., 1960. The Fe-As-S system–Phase relations and applications. Economic Geology 55, 1345–1381. https://doi.org/10.2113/gsecongeo.55.7.1345.

Cook, N.J., Chryssoulis, S.L., 1990. Concentrations of invisible gold in the common sulfides. The Canadian Mineralogist 28, 1–16.

Cook, N.J., Ciobanu, C.L., Meria, D., Silcock, D., Wade, B., 2013. Arsenopyrite-Pyrite Association in an Orogenic Gold Ore: Tracing Mineralization History from Textures and Trace Elements. Economic Geology 108, 1273–1283. https://doi.org/10.2113/econgeo.108.6.1273.

Deditius, A.P., Reich, M., Kesler, S.E., Utsunomiya, S., Chryssoulis, S.L., Walshe, J., Ewing, R.C., 2014. The coupled geochemistry of Au and As in pyrite from hydrothermal ore deposits. Geochimica et Cosmochimica Acta 140, 644–670. https://doi.org/10.1016/j.gca.2014.05.045.

Deditius, A.P., Utsunomiya, S., Ewing, R.C., Kesler, S.E., 2009. Nanoscale "liquid" inclusions of As-Fe-S in arsenian pyrite. American Mineralogist 94, 391–394. https://doi.org/10.2138/am.2009.3116.

Deditius, A.P., Utsunomiya, S., Reich, M., Kesler, S.E., Ewing, R.C., Hough, R., Walshe, J., 2011. Trace metal nanoparticles in pyrite. Ore Geology Reviews 42, 32–46. https://doi.org/10.1016/j.oregeorev.2011.03.003.

Deditius, A.P., Utsunomiya, S., Renock, D., Ewing, R.C., Ramana, C.V., Becker, U., Kesler, S.E., 2008. A proposed new type of arsenian pyrite: Composition, nanostructure and geological significance. Geochimica et Cosmochimica Acta 72, 2919–2933. https://doi.org/10.1016/j.gca.2008.03.014.

Deng, T., Xu, D., Chi, G., Wang, Z., Jiao, Q., Ning, J., Dong, G., Zou, F., 2017. Geology, geochronology, geochemistry and ore genesis of the Wangu gold deposit in northeastern Hunan Province, Jiangnan Orogen, South China. Ore Geology Reviews 88, 619–637. https://doi.org/10.1016/j.oregeorev.2017.01.012.

Deol, S., Deb, M., Large, R.R., Gilbert, S., 2012. LA-ICPMS and EPMA studies of pyrite, arsenopyrite and loellingite from the Bhukia-Jagpura gold prospect, southern Rajasthan, India: Implications for ore genesis and gold remobilization. Chemical Geology 326–327, 72–87. https://doi.org/10.1016/j.chemgeo.2012.07.017.

El-Bouseily, A.M., El-Dahhar, M.A., Arslan, A.I., 1985. Ore-microscopic and geochemical characteristics of gold-bearing sulfide minerals, El Sid Gold mine, Eastern Desert. Egypt. Mineral. Deposita 20, 194–200. https://doi.org/10.1007/BF00204565.

Evans, K.A., Phillips, G.N., Powell, R., 2006. Rock-Buffering of Auriferous Fluids in Altered Rocks Associated with the Golden Mile-Style Mineralization, Kalgoorlie Gold Field, Western Australia. Economic Geology 101, 805–817. https://doi.org/10.2113/gsecongeo.101.4.805.

Ferry, J.M., 1981. Petrology of graphitic sulfide-rich schists from South-central Maine: an example of desulfidation during prograde regional metamorphism. American Mineralogist 66, 908–930.

Fleet, M.E., Chryssoulis, S.L., Davidson, R., Weisener, C.G., Maclean, P.J., 1993. Arsenian pyrite from gold deposits: Au and As distribution investigated by SIMS and EMP, and color staining and surface oxidation by XPS and LIMS. Canadian Mineralogist 31, 1–17.

Fleet, M.E., Maclean, P.J., Barbier, J., 1988. Oscillatory-zoned As-bearing pyrite from strata-bound and stratiform gold deposits: an indicator of ore-fluid evolution. Economic Geology Monograph 6, 356–362.

Fleet, M.E., Mumin, A.H., 1997. Gold-bearing arsenian pyrite and marcasite and arsenopyrite from Carlin Trend gold deposits and laboratory synthesis. American Mineralogist 82, 182–193.

George, L.L., Cook, N.J., Ciobanu, C.L., 2016. Partitioning of trace elements in co-crystallized sphalerite–galena–chalcopyrite hydrothermal ores. Ore Geology Reviews 77, 97–116. https://doi.org/10.1016/j.oregeorev.2016.02.009.

Gilbert, S.E., Danyushevsky, L.V., Goemann, K., Death, D., 2014a. Fractionation of sulphur relative to iron during laser ablation-ICP-MS analyses of sulphide minerals: Implications for quantification. Journal of Analytical Atomic Spectrometry 29, 1024–1033. https://doi.org/10.1039/c4ja00012a.

Gilbert, S.E., Danyushevsky, L.V., Rodemann, T., Shimizu, N., Gurenko, A., Meffre, S., Thomas, H., Large, R.R., Death, D., 2014b. Optimisation of laser parameters for the analysis of sulphur isotopes in sulphide minerals by laser ablation ICP-MS. J. Anal. At. Spectrom. 29, 1042–1051. https://doi.org/10.1039/C4JA00011K.

Gopon, P., Douglas, J.O., Auger, M.A., Hansen, L., Wade, J., Cline, J.S., Robb, L.J., Moody, M.P., 2019. A Nanoscale Investigation of Carlin-Type Gold Deposits: An Atom-Scale Elemental and Isotopic Perspective. Economic Geology 114, 1123–1133. https://doi.org/10.5382/econgeo.4676.

Gregory, D.D., Large, R.R., Halpin, J.A., Baturina, E.L., Lyons, T.W., Wu, S., Danyushevsky, L., Sack, P.J., Chappaz, A., Maslennikov, V.V., Bull, S.W., 2015. Trace element content of sedimentary pyrite in black shales. Economic Geology 110, 1389–1410. https://doi.org/10.2113/econgeo.110.6.1389.

Hem, S.R., Makovicky, E., 2004a. The system Fe–Co–Ni–As–S. I. Phase relations in the (Fe Co, Ni)As0.5S1.5 section at 650° and 500°C. Can Mineral 42, 43–62. https://doi.org/10.2113/gscanmin.42.1.43.

Hem, S.R., Makovicky, E., 2004b. The system Fe–Co–Ni–As–S. II. Phase relations in the (Fe Co, Ni)As1.5S0.5 section at 650° and 500°C. Can Mineral 42, 63–86. https://doi.org/10.2113/gscanmin.42.1.63.

Hou, L., Peng, H., Ding, J., Zhang, J., Zhu, S., Wu, S., Wu, Y., Ouyang, H., 2016. Textures and In Situ Chemical and Isotopic Analyses of Pyrite, Huijiabao Trend, Youjiang Basin, China: Implications for Paragenesis and Source of Sulfur. Economic Geology 111, 331–353. https://doi.org/10.2113/econgeo.111.2.331.

Hu, X., Zeng, G., Zhang, Z., Li, W., Liu, W., Gong, Y., Yao, S., 2018. Gold mineralization associated with Emeishan basaltic rocks: Mineralogical, geochemical, and isotopic evidences from the Lianhuashan ore field, southwestern Guizhou Province, China. Ore Geology Reviews 95, 604–619. https://doi.org/10.1016/j.oregeorev.2018.03.016.

Hurtig, N.C., Heinrich, C.A., Driesner, T., Herrmann, W., Wall, V., Mathison, I., 2014. Fluid Evolution and Uranium (-Mo-F) Mineralization at the Maureen Deposit (Queensland, Australia): Unconformity-Related Hydrothermal Ore Formation with a Source in the Volcanic Cover Sequence. Economic Geology 109, 737–773. https://doi.org/10.2113/econgeo.109.3.737.

Huston, D.L., Sie, S.H., Suter, G.F., Cooke, D.R., Both, R.A., 1995. Trace elements in sulfide minerals from eastern Australian volcanic- hosted massive sulfide deposits: part I. Proton microprobe analyses of pyrite, chalcopyrite, and sphalerite, and part II. Selenium levels in pyrite: comparison with δ 34S values and implications for the source of sulfur in volcanogenic hydrothermal systems. Economic Geology 90, 1167–1196. https://doi.org/10.2113/gsecongeo.90.5.1167.

Jha, V., Singh, S., Venkatesh, A.S., 2015. Invisible gold occurrence within the quartz reef pyrite of Babaikundi area, North Singhbhum fold-and-thrust belt, Eastern Indian Shield: Evidence from petrographic, SEM and EPMA studies. Ore Geology Reviews 65, 426–432. https://doi.org/10.1016/j.oregeorev.2014.10.003.

Kiseeva, E.S., Wood, B.J., 2013. A simple model for chalcophile element partitioning between sulphide and silicate liquids with geochemical applications. Earth and Planetary Science Letters 383, 68–81. https://doi.org/10.1016/j.epsl.2013.09.034.

Kishima, N., 1989. A thermodynamic study on the pyrite-pyrrhotite-magnetite-water system at 300–500°C with relevance to the fugacity/concentration quotient of aqueous H2S. Geochimica et Cosmochimica Acta 53, 2143–2155. https://doi.org/10.1016/0016-7037(89)90340-2.

Korsakov, A.V., Perraki, M., Zedgenizov, D.A., Bindi, L., Vandenabeele, P., Suzuki, A., Kagi, H., 2010. Diamond-Graphite Relationships in Ultrahigh-pressure Metamorphic Rocks from the Kokchetav Massif, Northern Kazakhstan. Journal of Petrology 51, 763–783. https://doi.org/10.1093/petrology/egq001.

Kovalev, K.R., Kalinin, Y., Naumov, E.A., Kolesnikova, M.K., Korolyuk, V.N., 2011. Gold-bearing arsenopyrite in eastern Kazakhstan gold-sulfide deposits. Russian Geology and Geophysics 52, 178–192.

Kovalev, K.R., Kalinin, Y.A., Naumov, E.A., Pirajno, F., Borisenko, A.S., 2009. A mineralogical study of the Suzdal sediment-hosted gold deposit, Eastern Kazakhstan: Implications for ore genesis. Ore Geology Reviews 35, 186–205. https://doi.org/10.1016/j.oregeorev.2008.11.007.

Kretschmar, U., Scott, S.D., 1976. Phase relations involving arsenopyrite in the system Fe-As-S and their application. Can Mineral 14, 364–386.

Kusebauch, C., Gleeson, S.A., Oelze, M., 2019. Coupled partitioning of Au and As into pyrite controls formation of giant Au deposits. Science. Advances 5, eaav5891. https://doi.org/10.1126/sciadv.aav5891.

Kusebauch, C., Oelze, M., Gleeson, S.A., 2018. Partitioning of arsenic between hydrothermal fluid and pyrite during experimental siderite replacement. Chemical Geology 500, 136–147. https://doi.org/10.1016/j.chemgeo.2018.09.027.

Large, R., Thomas, H., Craw, D., Henne, A., Henderson, S., 2012. Diagenetic pyrite as a source for metals in orogenic gold deposits, Otago Schist, New Zealand. New Zealand Journal of Geology and Geophysics 55, 137–149.

Large, R.R., Bull, S.W., Maslennikov, V.V., 2011. A carbonaceous sedimentary source-rock model for Carlin-type and orogenic gold deposits. Economic Geology 106, 331–358. https://doi.org/10.2113/econgeo.106.3.331.

Large, R.R., Gregory, D.D., Steadman, J.A., Tomkins, A.G., Lounejeva, E., Danyushevsky, L.V., Halpin, J.A., Maslennikov, V., Sack, P.J., Mukherjee, I., Berry, R., Hickman, A., 2015a. Gold in the oceans through time. Earth and Planetary Science Letters 428, 139–150. https://doi.org/10.1016/j.epsl.2015.07.026.

Large, R.R., Halpin, J.A., Lounejeva, E., Danyushevsky, L.V., Maslennikov, V.V., Gregory, D., Sack, P.J., Haines, P.W., Long, J.A., Makoundi, C., Stepanov, A.S., 2015b. Cycles of nutrient trace elements in the Phanerozoic ocean. Gondwana Research 28, 1282–1293. https://doi.org/10.1016/j.gr.2015.06.004.

Large, R.R., Maslennikov, V.V., 2020. Invisible Gold Paragenesis and Geochemistry in Pyrite from Orogenic and Sediment-Hosted Gold Deposits. Minerals 10, 339. https://doi.org/10.3390/min10040339.

Large, R.R., Maslennikov, V.V., Robert, F., Danyushevsky, L.V., Chang, Z., 2007. Multistage sedimentary and metamorphic origin of pyrite and gold in the giant Sukhoi Log deposit, Lena Gold Province, Russia. Economic Geology 102, 1233–1267.

Large, R.R., Mukherjee, I., Gregory, D.D., Steadman, J.A., Maslennikov, V.V., Meffre, S., 2017. Ocean and Atmosphere Geochemical Proxies Derived from Trace Elements in Marine Pyrite: Implications for Ore Genesis in Sedimentary Basins. Economic Geology 112, 423–450. https://doi.org/10.2113/econgeo.112.2.423.

Le Pape, P., Marc, B., Amélie, J., Jean-Pascal, R., Manoj, D., Guillaume, M., Delphine, C., 2018. Local environment of arsenic in sulfide minerals: insights from high-resolution X-ray spectroscopies, and first-principles calculations at the As K-edge. J. Anal. At. Spectrom. 33, 2070–2082. https://doi.org/10.1039/C8JA00272J.

Li, N., Deng, J., Yang, L.-Q., Goldfarb, R.J., Zhang, C., Marsh, E., Lei, S.-B., Koenig, A., Lowers, H., 2014. Paragenesis and geochemistry of ore minerals in the epizonal gold deposits of the Yangshan gold belt, West Qinling, China. Miner Deposita 49, 427–449. https://doi.org/10.1007/s00126-013-0498-8.

Li, W., Cook, N.J., Xie, G.-Q., Mao, J.-W., Ciobanu, C.L., Li, J.-W., Zhang, Z.-Y., 2019. Textures and trace element signatures of pyrite and arsenopyrite from the Gutaishan Au–Sb deposit, South China. Miner Deposita 54, 591–610. https://doi.org/10.1007/s00126-018-0826-0.

Li, X.-H., Fan, H.-R., Yang, K.-F., Hollings, P., Liu, X., Hu, F.-F., Cai, Y.-C., 2018. Pyrite textures and compositions from the Zhuangzi Au deposit, southeastern North China Craton: implication for ore-forming processes. Contrib Mineral Petrol 173, 73. https://doi.org/10.1007/s00410-018-1501-2.

Liu, A.-L., Jiang, M.-R., Ulrich, T., Zhang, J., Zhang, X.-J., 2018. Ore genesis of the Bake gold deposit, southeastern Guizhou province, China: Constraints from mineralogy, in-situ trace element and sulfur isotope analysis of pyrite. Ore Geology Reviews 102, 740–756. https://doi.org/10.1016/j.oregeorev.2018.09.018.

Massalski, T.B., 1989. Phase diagrams in materials science. MTB 20, 445–473. https://doi.org/10.1007/BF02654595.

McClenaghan, S.H., Lentz, D.R., Martin, J., Diegor, W.G., 2009. Gold in the Brunswick No. 12 volcanogenic massive sulfide deposit, Bathurst Mining Camp, Canada: Evidence from bulk ore analysis and laser ablation ICP—MS data on sulfide phases. Miner Deposita 44, 523–557. https://doi.org/10.1007/s00126-009-0233-7.

Möller, P., Kersten, G., 1994. Electrochemical accumulation of visible gold on pyrite and arsenopyrite surfaces. Mineral. Deposita 29, 404–413. https://doi.org/10.1007/BF01886958.

Morey, A.A., Tomkins, A.G., Bierlein, F.P., Weinberg, R.F., Davidson, G.J., 2008. Bimodal Distribution of Gold in Pyrite and Arsenopyrite: Examples from the Archean Boorara and Bardoc Shear Systems, Yilgarn Craton, Western Australia. Economic Geology 103, 599–614. https://doi.org/10.2113/gsecongeo.103.3.599.

Morishita, Y., Hammond, N.Q., Momii, K., Konagaya, R., Sano, Y., Takahata, N., Ueno, H., 2019. Invisible Gold in Pyrite from Epithermal, Banded-Iron-Formation-Hosted, and Sedimentary Gold Deposits: Evidence of Hydrothermal Influence. Minerals 9, 447. https://doi.org/10.3390/min9070447.

Morishita, Y., Shimada, N., Shimada, K., 2018. Invisible gold in arsenian pyrite from the high-grade Hishikari gold deposit, Japan: Significance of variation and distribution of Au/As ratios in pyrite. Ore Geology Reviews 95, 79–93. https://doi.org/10.1016/j.oregeorev.2018.02.029.

Mumin, A.H., Fleet, M.E., Chryssoulis, S.L., 1994. Gold mineralization in As-rich mesothermal gold ores of the Bogosu-Prestea mining district of the Ashanti Gold Belt, Ghana: remobilization of "invisible" gold. Mineral. Deposita 29, 445–460. https://doi.org/10.1007/BF00193506.

Murzin, V.V., Naumov, E.A., Azovskova, O.B., Varlamov, D.A., Rovnushkin, M.Y., Pirajno, F., 2017. The Vorontsovskoe Au-Hg-As ore deposit (Northern Urals, Russia): Geological setting, ore mineralogy, geochemistry, geochronology and genetic model. Ore Geology Reviews, Overview of mineral deposits in the Urals 85, 271–298. https://doi.org/10.1016/j.oregeorev.2016.10.037.

Palenik, C.S., Utsunomiya, S., Reich, M., Kesler, S.E., Wang, L., Ewing, R.C., 2004. "Invisible" gold revealed: Direct imaging of gold nanoparticles in a Carlin-type deposit. American Mineralogist 89, 1359–1366.

Perfetti, E., Pokrovski, G.S., Ballerat-Busserolles, K., Majer, V., Gibert, F., 2008. Densities and heat capacities of aqueous arsenious and arsenic acid solutions to 350°C and 300bar, and revised thermodynamic properties of As(OH)3∘(aq), AsO(OH)3∘(aq) and iron sulfarsenide minerals. Geochimica et Cosmochimica Acta 72, 713–731. https://doi.org/10.1016/j.gca.2007.11.017.

Peterson, E.C., Mavrogenes, J.A., 2014. Linking high-grade gold mineralization to earthquake-induced faultvalve processes in the Porgera gold deposit, Papua New Guinea. Geology 42, 383–386. https://doi.org/10.1130/G35286.1.

Phillips, G.N., Powell, R., 2010. Formation of gold deposits: a metamorphic devolatilization model. Journal of Metamorphic Geology 28, 689–718. https://doi.org/10.1111/j.1525-1314.2010.00887.x.

Pires, G.L.C., Renac, C., Bongiolo, E.M., Neumann, R., Barats, A., 2019. P-T–X conditions on the genesis of orogenic Au (As, Bi, Ag) deposit in metasedimentary rocks of the Buracão Area, Araí Group, Brasília Fold Belt, Brazil. Ore Geology Reviews 105, 163–182. https://doi.org/10.1016/j.oregeorev.2018.12.017.

Pitcairn, I.K., Craw, D., Teagle, D.A.H., 2014. Metabasalts as sources of metals in orogenic gold deposits. Miner Deposita 50, 373–390. https://doi.org/10.1007/s00126-014-0547-y.

Pitcairn, I.K., Olivo, G.R., Teagle, D.A.H., Craw, D., 2010. Sulfide evolution during prograde metamorphism of the Otago and Alpine schists, New Zealand. Canadian Mineralogist 48, 1267–1295. https://doi.org/10.3749/canmin.48.5.1267.

Pitcairn, I.K., Skelton, A.D.L., Wohlgemuth-Ueberwasser, C.C., 2015. Mobility of gold during metamorphism of the Dalradian in Scotland. Lithos, Geochemistry and Earth Systems – A Special Issue in Memory of Robert Kerrich 233, 69–88. https://doi.org/10.1016/j.lithos.2015.05.006.

Pitcairn, I.K., Teagle, D.A.H., Craw, D., Olivo, G.R., Kerrich, R., Brewer, T.S., 2006. Sources of Metals and Fluids in Orogenic Gold Deposits: Insights from the Otago and Alpine Schists, New Zealand. Economic Geology 101, 1525–1546. https://doi.org/10.2113/gsecongeo.101.8.1525.

Pokrovski, G., Gout, R., Schott, J., Zotov, A., Harrichoury, J.-C., 1996. Thermodynamic properties and stoichiometry of As (III) hydroxide complexes at hydrothermal conditions. Geochimica et Cosmochimica Acta 60, 737–749. https://doi.org/10.1016/0016-7037(95)00427-0.

Pokrovski, G.S., Kara, S., Roux, J., 2002. Stability and solubility of arsenopyrite, FeAsS, in crustal fluids. Geochimica et Cosmochimica Acta 66, 2361–2378. https://doi.org/10.1016/S0016-7037(02)00836-0.

Pokrovski, G.S., Kokh, M.A., Proux, O., Hazemann, J.-L., Bazarkina, E.F., Testemale, D., Escoda, C., Boiron, M.-C., Blanchard, M., Aigouy, T., Gouy, S., de Parseval, P., Thibaut, M., 2019. The nature and partitioning of invisible gold in the pyrite-fluid system. Ore Geology Reviews 109, 545–563. https://doi.org/10.1016/j.oregeorev.2019.04.024.

Qian, G., Brugger, J., Testemale, D., Skinner, W., Pring, A., 2013. Formation of As(II)-pyrite during experimental replacement of magnetite under hydrothermal conditions. Geochimica et Cosmochimica Acta 100, 1–10. https://doi.org/10.1016/j.gca.2012.09.034.

Qian, G., Xia, F., Brugger, J., Skinner, W.M., Bei, J., Chen, G., Pring, A., 2011. Replacement of pyrrhotite by pyrite and marcasite under hydrothermal conditions up to 220 °C: An experimental study of reaction textures and mechanisms. American Mineralogist 96, 1878–1893. https://doi.org/10.2138/am.2011.3691.

Rajabpour, S., Behzadi, M., Jiang, S.-Y., Rasa, I., Lehmann, B., Ma, Y., 2017. Sulfide chemistry and sulfur isotope characteristics of the Cenozoic volcanic-hosted Kuh-Pang copper deposit, Saveh county, northwestern central Iran. Ore Geology Reviews 86, 563–583. https://doi.org/10.1016/j.oregeorev.2017.03.001.

Reeder, R.J., Paquette, J., 1989. Sector zoning in natural and synthetic calcites. Sedimentary Geology 65, 239–247. https://doi.org/10.1016/0037-0738(89)90026-2.

Reich, M., Becker, U., 2006. First-principles calculations of the thermodynamic mixing properties of arsenic incorporation into pyrite and marcasite. Chemical Geology 225, 278–290.

Reich, M., Kesler, S.E., Utsunomiya, S., Palenik, C.S., Chryssoulis, S.L., Ewing, R.C., 2005. Solubility of gold in arsenian pyrite. Geochimica et Cosmochimica Acta 69, 2781–2796.

Salier, B.P., Groves, D.I., McNaughton, N.J., Fletcher, I.R., 2005. Geochronological and Stable Isotope Evidence for Widespread Orogenic Gold Mineralization from a Deep-Seated Fluid Source at ca 2.65 Ga in the Laverton Gold Province. Western Australia. Economic Geology 100, 1363–1388. https://doi.org/10.2113/gsecongeo.100.7.1363.

Salvi, S., Velásquez, G., Miller, J.M., Béziat, D., Siebenaller, L., Bourassa, Y., 2016. The Pampe gold deposit (Ghana): Constraints on sulfide evolution during gold mineralization. Ore Geology Reviews 78, 673–686. https://doi.org/10.1016/j.oregeorev.2015.11.006.

Savage, K.S., Tingle, T.N., O'Day, P.A., Waychunas, G.A., Bird, D.K., 2000. Arsenic speciation in pyrite and secondary weathering phases, Mother Lode Gold District, Tuolumne County, California. Applied Geochemistry 15, 1219–1244.

Shao, Y.-J., Wang, W.-S., Liu, Q.-Q., Zhang, Y., 2018. Trace Element Analysis of Pyrite from the Zhengchong Gold Deposit, Northeast Hunan Province, China: Implications for the Ore-Forming Process. Minerals 8, 262. https://doi.org/10.3390/min8060262.

Sharp, Z.D., Essene, E.J., Kelly, W.C., 1985. A re-examination of the arsenopyrite geothermometer; pressure considerations and applications to natural assemblages. Can Mineral 23, 517–534.

Shtukenberg, A.G., Punin, Y.O., Artamonova, O.I., 2009. Effect of crystal composition and growth rate on sector zoning in solid solutions grown from aqueous solutions. Mineralogical Magazine 73, 385–398. https://doi.org/10.1180/minmag.2009.073.3.385.

Simon, G., Huang, H., Penner-Hahn, J.E., Kesler, S.E., Kao, L.-S., 1999a. Oxidation state of gold and arsenic in gold-bearing arsenian pyrite. American Mineralogist 84, 1071–1079.

Simon, G., Kesler, S.E., Chryssoulis, S., 1999b. Geochemistry and textures of gold-bearing arsenian pyrite, Twin Creeks, Nevada; implications for deposition of gold in carlin-type deposits. Economic Geology 94, 405–421. https://doi.org/10.2113/gsecongeo.94.3.405.

Slim-Shimi, N., Moëlo, Y., Tlig, S., Lévy, C., 1996. Sulfide geochemistry and genesis of Chouichia and Ain el Bey copper deposits in northwestern Tunisia. Mineral. Deposita 31, 188–200. https://doi.org/10.1007/BF00204026.

Smith, R.N., Huston, D.L., 1992. Distribution and association of selected trace elements at the Rosebery Deposit, Tasmania. Economic Geology 87, 706–719. https://doi.org/10.2113/gsecongeo.87.3.706.

Starr, P.G., Pattison, D.R.M., 2019. Equilibrium and disequilibrium processes across the greenschist–amphibolite transition zone in metabasites. Contrib Mineral Petrol 174, 18. https://doi.org/10.1007/s00410-019-1553-y.

Steadman, J.A., Large, R.R., 2016. Synsedimentary, Diagenetic, and Metamorphic Pyrite, Pyrrhotite, and Marcasite at the Homestake BIF-Hosted Gold Deposit, South Dakota, USA: Insights on Au-As Ore Genesis from Textural and LA-ICP-MS Trace Element Studies. Economic Geology 111, 1731–1752. https://doi.org/10.2113/econgeo.111.7.1731.

Stepanov, A.S., 2021. A review of the geochemical changes occurring during metamorphic devolatilization of metasedimentary rocks. Chemical Geology 120080. https://doi.org/10.1016/j.chemgeo.2021.120080.

Stepanov, A.S., 2019. Arsenic evolution as a tool for understanding formation of pyritic gold ores: COMMENT. Geology 47, e491. https://doi.org/10.1130/G46794C.1.

Stepanov, A.S., Danyushevsky, L.V., Large, R.R., Mukherjee, I., Zhukova, I.A., 2020. Deconvolution of the composition of fine-grained pyrite in sedimentary matrix by regression of time-resolved LA-ICP-MS data. American Mineralogist 105, 820–832. https://doi.org/10.2138/am-2020-7202.

Sung, Y.-H., Brugger, J., Ciobanu, C.L., Pring, A., Skinner, W., Nugus, M., 2009. Invisible gold in arsenian pyrite and arsenopyrite from a multistage Archaean gold deposit: Sunrise Dam, Eastern Goldfields Province, Western Australia. Miner Deposita 44, 765–791. https://doi.org/10.1007/s00126-009-0244-4.

Sykora, S., Cooke, D.R., Meffre, S., Stephanov, A.S., Gardner, K., Scott, R., Selley, D., Harris, A.C., 2018. Evolution of Pyrite Trace Element Compositions from Porphyry-Style and Epithermal Conditions at the Lihir Gold Deposit: Implications for Ore Genesis and Mineral Processing. Economic Geology 113, 193–208. https://doi.org/10.5382/econgeo.2018.4548.

Tang, Q., Di, P., Yu, M., Bao, J., Zhao, Y., Liu, D., Wang, Y., 2019. Mineralogy and Geochemistry of Pyrite and Arsenopyrite from the Zaozigou Gold Deposit in West

Qinling Orogenic Belt, Central China: Implications for Ore Genesis. Resource Geology 69, 314–332. https://doi.org/10.1111/rge.12203.
Tardani, D., Reich, M., Deditius, A.P., Chryssoulis, S., Sánchez-Alfaro, P., Wrage, J., Roberts, M.P., 2017. Copper-arsenic decoupling in an active geothermal system: a link between pyrite and fluid composition. Geochimica et Cosmochimica Acta 204, 179–204. https://doi.org/10.1016/j.gca.2017.01.044.
Tauson, V.L., 1999. Gold solubility in the common gold-bearing minerals: Experimental evaluation and application to pyrite. European Journal of Mineralogy 11, 937–948. https://doi.org/10.1127/ejm/11/6/0937.
Tauson, V.L., Kravtsova, R.G., Smagunov, N.V., Spiridonov, A.M., Grebenshchikova, V.I., Budyak, A.E., 2014. Structurally and superficially bound gold in pyrite from deposits of different genetic types. Russian Geology and Geophysics, Geochemistry of Magmatic and Ore-Forming Processes in the Central Asian Orogenic Belt 55, 273–289. https://doi.org/10.1016/j.rgg.2014.01.011.
Tauson, V.L., Pastushkova, T.M., Babkin, D.N., Krasnoshchekova, T.S., Lustenberg, E.E., 2010. The effect of the crystal size in sample on the trace-element concentration. Russian Geology and Geophysics 51, 764–773. https://doi.org/10.1016/j.rgg.2010.06.004.
Thomas, H.V., Large, R.R., Bull, S.W., Maslennikov, V., Berry, R.F., Fraser, R., Froud, S., Moye, R., 2011. Pyrite and pyrrhotite textures and composition in sediments, laminated quartz veins, and reefs at Bendigo gold mine, Australia: Insights for ore genesis. Economic Geology 106, 1–31.
Tiller, W.A., Ahn, K.-S., 1980. Interface field effects on solute redistribution during crystallization. Journal of Crystal Growth 49, 483–501. https://doi.org/10.1016/0022-0248(80)90123-2.
Tomkins, A., Pattison, D., Frost, R., 2007. On the initiation of metamorphic sulfide anatexis.
Tomkins, A.G., 2010. Windows of metamorphic sulfur liberation in the crust: Implications for gold deposit genesis. Geochimica et Cosmochimica Acta 74, 3246–3259. https://doi.org/10.1016/j.gca.2010.03.003.
Tomkins, A.G., Frost, B.R., Pattison, D.R.M., 2006. Arsenopyrite melting during metamorphism of sulfide ore deposits. Canadian Mineralogist 44, 1045–1062. https://doi.org/10.2113/gscanmin.44.5.1045.
Toulmin, P., Barton, P.B., 1964. A thermodynamic study of pyrite and pyrrhotite. Geochimica et Cosmochimica Acta 28, 641–671. https://doi.org/10.1016/0016-7037(64)90083-3.
Turnbull, D., 1981. Metastable structures in metallurgy. Metallurgical Transactions B 12, 217–230. https://doi.org/10.1007/BF02654454.
van Hinsberg, V.J., King, J., Marin, A.G., Clark, J.R., Williams-Jones, A.E., 2010. A new pyrite thermometer based on inter-sector element partitioning.
Vilor, N.V., Kaz'min, L.A., Pavlova, L.A.,, 2014. Aresenopyrite-pyrite paragenesis in gold deposits (thermodynamic modeling). Russian Geology and Geophysics 55, 824–841. https://doi.org/10.1016/j.rgg.2014.06.003.
Watson, E.B., 2004. A conceptual model for near-surface kinetic controls on the trace-element and stable isotope composition of abiogenic calcite crystals1. Geochimica et Cosmochimica Acta 68, 1473–1488. https://doi.org/10.1016/j.gca.2003.10.003.
Watson, E.B., 1996. Surface enrichment and trace-element uptake during crystal growth. Geochimica et Cosmochimica Acta 60, 5013–5020. https://doi.org/10.1016/S0016-7037(96)00299-2.
Watson, E.B., Cherniak, D.J., Frank, E.A., 2009. Retention of biosignatures and mass-independent fractionations in pyrite: Self-diffusion of sulfur. Geochimica et Cosmochimica Acta 73, 4792–4802. https://doi.org/10.1016/j.gca.2009.05.060.
Wells, J.D., Mullens, T.E., 1973. Gold-Bearing Arsenian Pyrite Determined by Microprobe Analysis, Cortez and Carlin Gold mines, Nevada. Economic Geology 68, 187–201. https://doi.org/10.2113/gsecongeo.68.2.187.
Winderbaum, L., Ciobanu, C.L., Cook, N.J., Paul, M., Metcalfe, A., Gilbert, S., 2012. Multivariate Analysis of an LA-ICP-MS Trace Element Dataset for Pyrite. Math Geosci 44, 823–842. https://doi.org/10.1007/s11004-012-9418-1.
Wu, Y.-F., Evans, K., Li, J.-W., Fougerouse, D., Large, R.R., Guagliardo, P., 2019a. Metal remobilization and ore-fluid perturbation during episodic replacement of auriferous pyrite from an epizonal orogenic gold deposit. Geochimica et Cosmochimica Acta 245, 98–117. https://doi.org/10.1016/j.gca.2018.10.031.
Wu, Y.-F., Fougerouse, D., Evans, K., Reddy, S.M., Saxey, D.W., Guagliardo, P., Li, J.-W., 2019b. Gold, arsenic, and copper zoning in pyrite: A record of fluid chemistry and growth kinetics. Geology 47, 641–644. https://doi.org/10.1130/G46114.1.
Xing, Y., Brugger, J., Tomkins, A., Shvarov, Y., 2019a. Arsenic evolution as a tool for understanding formation of pyritic gold ores. Geology 47, 335–338. https://doi.org/10.1130/G45708.1.
Xing, Y., Brugger, J., Tomkins, A., Shvarov, Y., 2019b. Arsenic evolution as a tool for understanding formation of pyritic gold ores: REPLY. Geology 47, e492. https://doi.org/10.1130/G46938Y.1.
Zacharias, J., Frýda, J., Paterová, B., Mihaljevič, M., 2004. Arsenopyrite and As-bearing pyrite from the Roudný deposit, Bohemian Massif. Mineralogical Magazine 68, 31–46. https://doi.org/10.1180/0026461046810169.
Zhang, G., Xue, C., Chi, G., Liu, J., Zhao, X., Zu, B., Zhao, Y., 2017. Multiple-stage mineralization in the Sawayaerdun orogenic gold deposit, western Tianshan, Xinjiang: Constraints from paragenesis, EMPA analyses, Re–Os dating of pyrite (arsenopyrite) and U-Pb dating of zircon from the host rocks. Ore Geology Reviews P1, 326–341. https://doi.org/10.1016/j.oregeorev.2016.10.038.
Zhang, J., Li, L., Gilbert, S., Liu, J.-J., Shi, W.-S., 2014. LA–ICP–MS and EPMA studies on the Fe–S–As minerals from the Jinlongshan gold deposit, Qinling Orogen, China: implications for ore-forming processes. Geological Journal 49, 482–500. https://doi.org/10.1002/gj.2594.
Zoheir, B., Emam, A., Pitcairn, I.K., Boskabadi, A., Lehaye, Y., Cooper, M.J., 2019. Trace elements and isotope data of the Um Garayat gold deposit, Wadi Allaqi district. Egypt. Miner Deposita 54, 101–116. https://doi.org/10.1007/s00126-018-0807-3.